EVALUATION OF BRINE DISPOSAL
FROM THE BRYAN MOUND SITE
OF THE STRATEGIC PETROLEUM RESERVE PROGRAM

Progress Report

Predisposal Studies

July 1979

by

Roy W. Hann, Jr., Program Director

Robert J. Case, Data Management

Mark E. Chittenden, Jr., Nekton Studies

Donald E. Harper, Jr., Benthic Studies

Francis J. Kelly, Jr., Physical Oceanography

James K. Lewis, Physical Oceanography

Larry D. McKinney, Benthic Studies

Robert E. Randall, Analysis of Discharge Plume

J. Frank Slowey, Sediment and Water Quality

and

Texas A&M Research Foundation

for

National Oceanic and Atmospheric Administration
Department of Commerce

SECTION I

PHYSICAL OCEANOGRAPHY

Introduction

The study area for the Bryan Mound Site of the Strategic Petroleum Reserve Program encompasses a nearshore area of approximately 640 km^2 and has an average depth of about 15 m (Fig. I-1). The region is characterized by a gently sloping bottom which results in water depths of only about 21 m as far out as 20 km.

Angelovic (1976) edited a review of the literature on the physical oceanographic characteristics of the Texas shelf, and the following nearshore properties have been discerned from his report. Along the Texas coast the freshest water is found nearshore east of Galveston, Texas throughout the year. The principle sources of the fresher waters are the Mississippi and Atchafalaya Rivers. The monthly mean salinities at shore tide stations show distinct spring minimums at Galveston and Port Aransas, Texas, but not at Brazos Santiago near Brownsville, Texas (see Fig. I-1). The authors' interpretation of the data is that normally there is a substantial penetration of low salinity water past Port Aransas but not beyond Brazos Santiago. This is a variable situation, however, and the May 1975 nearshore salinity records indicate a penetration of the fresher water as far south as Brownsville.

The review discusses data which indicate that in the nearshore waters from Galveston to Port Aransas the net flow is southwestward from October to mid-June and northeastward only in July and August. The data also indicate that a zone of convergence developes in waters of inner and middle-shelf areas and is most pronounced in spring. The nearshore location of the zone moves northeastward during spring through early summer, and the zone is

absent from October through February. The authors indicate that the convergence zone developes because of contrasting flows of nearshore water (flowing northeastward) and offshore water (flowing southwestward). It is also pointed out that intermittent upwelling is a probable cause for anomalously low nearshore sea water temperatures at Brazos Santiago during the summer. This feature is not seen in Galveston or Port Aransas.

With respect to hydrography, only a limited set of shelf data were available for consideration. In the nearshore areas for October through March there are temperature inversions and weak vertical temperature and salinity gradients. From March through May an initiation of thermal stratification occurs and a core of fresher water is found close to shore. In May 1964 this fresher water was found nearshore along the northeast and southwest ends of the Texas coast, but along the central Texas coast it was farther offshore in a thin narrow core. In June and July the thermal stratification intensified. By August the nearshore region was isothermal and isohaline.

The study undertaken here is a closer consideration of the nearshore hydrography and its variations with time. Fig. I-1 shows the grid of stations where monthly hydrographic data were collected from September 1977 through April 1979. Franceschini (1953) suggested that the circulation in the western Gulf is primarily wind driven, so hourly wind velocity measurements collected by NOAA's Data Buoy Office (NDBO) in the study area (Fig. I-1) were also used in this study. The NDBO meteorological package (for specifications see 1979 report prepared by Computer Sciences Corp for NDBO) was placed on an oil company platform, and a current meter/thermograph mooring was installed by Texas A&M University near the platform in approximately 17 m of water. Currents and temperatures were recorded at 2 m above the bottom and

3 to 4 meters below the surface. The currents were measured using Environmental Devices Corporation (ENDECO) type 105 tethered current meters which are designed for a wave zone environment. Temperature was recorded with General Oceanics Model 3070 thermographs.

Hydrographic Data

Beginning in September 1977 conductivity, temperature, and depth data have been collected at the surface (2 m below surface), mid-depth, and bottom (2 m above bottom) for the stations shown in Figure I-1. The exact stations monitored and frequency of cruises each month has varied depending upon weather, vessel downtime, and changes in project requirements. However, an effort was made to always sample along the transect coinciding with the pipeline and one normal to the pipeline through the diffuser site. These data have been used to plot vertical cross-sections of salinity, temperature and density (sigma-t) for the above mentioned transects.

During the first four months of the project a Beckman RS-5 induction salinometer was used to collect the salinity and temperature data. Beginning in February 1978, a Hydrolab TC-2 conductivity meter was used. Both instruments were calibrated against a Plessey laboratory salinometer in order to obtain salinity accuracies of approximately $0.3°/_{oo}$. The calibration procedures are outlined in detail in a previous report, Hann et al. (Feb. 1979).

Conductivity (C) data are converted to salinity (S) using the equation

$$S = .000848\ C^2 + .656\ C - 2.10$$

which is a curve fit to the conversion curve presented in the operating instructions for the Hydrolab Model TC-2 conductivity meter (Hydrolab, 1974). These salinities are used along with the temperature and depth to determine the density of the water. The density data are presented in the form of sigma-t (σ_t) which is defined as

$$\sigma_t = (\rho - 1.0) \times 10^{-3}\ gm/cm^3$$

The sigma-t values are computed from salinity, temperature, and depth data using the well known equations of LaFond (1951).

Salinity, Temperature and Sigma-t Data

Previous reports by Hann, et al. (Feb. 1979, July 1978, Feb. 1978) have described in detail the salinity, temperature, and sigma-t data collected from September 1977 through August 1978. The purpose of this subsection is to describe the hydrographic data collected from September 1978 through April 1979.

The September 25, 1978 temperature data (Figures I-2 and I-3) show a continuation of the nearly isothermal water column (28°C) described in August 1978 by Hann, et al. (Feb. 1979). The salinity data show a gradient of approximately 5°/$_{oo}$ from top to bottom except for the nearshore region (depths less than 9 m) where the water column is nearly isohaline. The August 1978 vertical salinity gradient was not as strong. The isopycnal lines are about 45 degrees from the horizontal and the sigma-t values vary from 17 to 20 x 10^{-3} gm/cm^3 at station 34 indicating a more stable, or more stratified, water column than that of the previous month. Thus the data show that during the summer months of 1978 the coastal waters in the study area were nearly isothermal and slightly stratified with the pycnocline near mid-depth.

In October 1978 (figures not shown), the water temperature of the study area decreased to 24°C but the water column remained isothermal. The variation in salinity and sigma-t was approximately 2°/$_{oo}$ and 1 x 10^{-3} gm/cm^3, respectively. The pycnocline was significantly weakened and had moved inshore. The weakening of the pycnocline and the stratification was expected for the fall months. The data of November 18, 1978 (Figures I-4 and I-5) are typical of the conditions for the fall 1978. These data show an isothermal and well-mixed water column with no pycnocline. The salinity and desnity increase with distance offshore, and the isopleths are vertical. The temperature

variation alongshore on a trasect through the diffuser site is less than 0.3°C (Figure I-5), and salinity and sigma-t vary by approximately 0.5°/$_{oo}$ and 0.5 x 10^{-3} gm/cm^3. In the fall of 1977, the November 17 data were not collected as far offshore, but they also showed a well-mixed condition. The data taken on December 18, 1978 (figures not shown) indicate a well-mixed condition similar to the November 1978 data. This is in contrast to the stratified conditions of December 1977 when the isopleths of salinity and sigma-t were horizontal.

In the winter months (Jan., Feb., Mar.) of 1979 the stratification increased and the isohalines and isopycnals were at an approximate 45° angle with the vertical. A typical example of the winter conditions is illustrated in Figures I-6 and I-7 which are the result of data collected on February 12, 1979. At the diffuser site (station 34) the salinity changes from 32°/$_{oo}$ to 35°/$_{oo}$ from top to bottom and sigma-t increases from 25 to 27 x 10^{-3} gm/cm^3. This indicates a stratified water column with the pycnocline occurring near mid-depth in the vicinity of the diffuser site. However, there is only a slight variation in temperature. There is an increase in the variation in the alongshore direction of salinity and sigma-t (0.8°/$_{oo}$ and 0.6 x 10^{-3} gm/cm^3) as shown in Figure I-7. Similar conditions were found on cruises in March 1979. The hydrographic data collected in the winter of 1979 have characteristics similar to those in 1978, but the pycnocline is not as strong as in December 1977, January 1978 and February 1978. The stratified water showed up a little later than in 1978 and presumably it occurred in January 1979 even though no data were collected during this month because of severe weather conditions.

During April 1979 strong stratification was detected. Figures I-8 and I-9 illustrate the data collected on April 16, 1979. The temperature decreases with distance offshore and a slight thermocline exists. The

ioshalines and isopycnals are nearly horizontal and a strong pycnocline exists at station 14 which is approximately 5 nautical miles offshore. At this location the salinity changes from 19°/$_{oo}$ to 32°/$_{oo}$ from top to bottom, and sigma-t increases from 12 x 10^{-3} to 22 x 10^{-3} gm/cm^3. The alongshore transect (Figure I-9) through the diffuser site (station 34) shows a small variation of temperature, salinity, and sigma-t (i.e. .4°C, .1°/$_{oo}$, .05 x 10^{-3} gm/cm^3 at bottom). The location of the pycnocline in the surface layer is evident in this figure. The conditions found during this month are much more severe than conditions found in the spring of 1978 which were typified by the May 25, 1978 data, Hann et al. (Feb. 1979).

The average variation of temperature, salinity, and sigma-t for the location of the diffuser station MM is shown in Figures I-10 and I-11. For these figures the data from the 2-3 cruises per month were average for the top, middle, and bottom depths. The diffuser site (station MM[34]) was first sampled in February 1978 and sampling was continued monthly except for January when high sea-state conditions caused cruise cancellations. The temperature was the lowest in February 1978 and 1979 with the warmer water located at the bottom which is typical for coastal waters. In March 1978 the water temperature warmed and the warmer water was found near the surface. This trend with a 2-3°C difference of top and bottom temperature continued through the spring and early summer. In July the difference in top and bottom temperatures was 1°C with the warmer temperature (30°C) at the surface. The water column was essentially isothermal during the months of August, September, October and November 1978, and a cooling of the water column began with temperature decreasing from 30°C in August to 22°C in November. During the winter months the surface temperature was cooler than the bottom water and the lowest temperature 9.5°C occurred in February 1979 at the surface. Again

this is typical behavior for coastal waters. In March 1979 the water column had warmed considerably to 12.5 °C on the surface. The temperature gradient had reversed such that the surface waters were warmer than the bottom and the temperature difference from top to bottom was about 1°C. This trend continued into April. The spring months in 1978 showed the same warming trend, but the top to bottom temperature difference in spring 1978 was about 3°C as compared to 1°C in 1979.

Figure I-10 also shows the variation of salinity at the diffuser site from February 1978 to April 1979. The overall salinity of the water column decreased from February to June 1978, and there was a large difference in salinity from top to bottom. The largest difference occurred in April when the surface salinity was 27.5°/$_{oo}$ and at the bottom it was 36°/$_{oo}$. The salinity increased in the early summer and reached a maximum value of 36.5°/$_{oo}$ at the bottom, and the variation of salinity from top to bottom decreased to 2°/$_{oo}$. In August the salinity decreased to 32.5°/$_{oo}$ on the surface and there was only a 1°/$_{oo}$ increase over the entire water column. In September the surface water freshened to a salinity of 29°/$_{oo}$ and a wide variation of 5°/$_{oo}$ existed over the depth. The fresher water disappeared over the next two months and the surface salinity increased to 33°/$_{oo}$ in November. The surface water began to freshen again in December and continued the trend through April 1979. The identical trend occurred in the winter and spring of 1978, but the variation of salinity over the depth was not as large as that in the same period of 1978.

The average variation of the density of the diffuser site is shown in Figure I-11 and is plotted in the familiar form of sigma-t. This plot shows the density of the water column generally decreased in the winter, spring, and early summer months, February to June 1978. In July the density increased and in August and September it decreased again. Then, the density increased again in October and continued this trend through February 1979. In March and April

1979 the density decreased in a similar way as was observed in the previous year. Over the 15 months of observations the water was stable with no density inversions. However, the pycnoclines moved between the top and bottom layers of water. An indication of the location of the pycnocline is determined by the separation of the mid-depth sigma-t line and the surface or bottom line. If the surface and mid-depth lines are further apart than the mid-depth and bottom lines, then the largest variation in density, or the pycnocline, was located in the surface layer. For example, the mid-depth and surface sigma-t in February 1978 differ by 2.75×10^{-3} gm/cm^3, and the mid-depth and bottom values are essentially identical. Therefore, the pycnocline is in the surface layer. The location of the pycnocline in the surface layer may not affect the brine plume but when it occurs in the bottom layer (i.e. June 1978) there will be a reduction in the turbulent mixing process.

As mentioned earlier the hydrographic stations have changed over the duration of the project due to changing of the diffuser sites, sea conditions and time constraints. In a previous report Hann et al. (Feb. 1979) a description of average temperature, salinity and sigma-t for all stations sampled was given. As a result averages were recomputed for stations 9, 12, 14, 16, 20, 33, MM, 36, and 39 which were common in most of the months. Therefore, a plot of these average values are shown in Figures I-12 and I-13. These figures show that the trends discussed for the diffuser site (station MM) are typical of the entire study area.

Stratification of the Water Column

A dimensionless parameter which is used to indicate stratification is the Richardson number. It considers the effects of both density and velocity gradients and is defined as

$$Ri = \frac{g}{\bar{\rho}} \frac{\frac{\Delta\rho}{\Delta z}}{\left(\frac{\Delta v}{\Delta z}\right)^2}$$

where $\bar{\rho}$ is the average density, V is the velocity, z is the depth, and g is the local acceleration due to gravity. When the Richardson number is positive the water column is stable, and the degree of stratification increases as the Richardson number increases. According to Officer (1976) the water column can be classified as well-mixed for $Ri \leq 0.1$, in transition for $0.1 < Ri \leq 10$, and stratified for $Ri > 10$.

The Richardson number was computed for the diffuser site (station MM) using the salinity, temperature, and depth data collected during monthly hydrographic surveys and current data collected at the same time with a Hydroproducts remote reading current meter. The water column was divided into surface and bottom layer. The bottom layer is of most interest because the far field portion of the negatively buoyant brine plume is expected to be in the bottom layer.

For the top layer the surface and middle depth data for salinity, temperature and depth (STD) were used to calculate $\bar{\rho}$ and $\Delta\rho/\Delta z$. The surface and mid-depth current data, which was a 2.5 minute vector average with a reading every 15 seconds, were used to calculate $\Delta v/\Delta z$. In the bottom layer a similar procedure was used to evaluate $\bar{\rho}$ and $\Delta\rho/\Delta z$ using mid-depth and bottom STD data. In the case of $\Delta v/\Delta z$, the bottom current was assumed to be zero at the sea floor interface.

The Richardson number data is plotted in Figure I-14 for each hydrographic survey beginning in February 1978 when station MM was first sampled. This figure shows that during the winter and early spring (Feb.-April 1978) the surface layer was stratified ($Ri>10$) on every cruise except one which was in the transition region ($0.1<Ri\leq10$). The bottom layer varied from being well-mixed ($Ri<0.1$) on one day in February to transitional on a day at the end of February. During the month of May 1978, the Richardson number in both layers were in the transitional region. In June there was no current data available because of equipment malfunction. For the remainder of the year the bottom layer was transitional with occasional days of well-mixed conditions. The surface layer was mostly transitional with occasional stratified and well-mixed days. No data were collected in January because of severe weather. The data in February and March of 1979 again showed the surface layer to be stratified and the bottom layer to be transitional. Unlike the previous year, the April data indicated that both layers were transitional with $Ri\simeq1$. In summary the Ri data indicates the bottom layer is transitional year round with occasional well-mixed conditions in winter and fall. The surface layer is generally stratified in the winter and spring months and transitional in the summer and fall months. The data also indicate large changes in Ri from cruise to cruise.

Temperature-Salinity Relationships

Since stratification was primarily a result of vertical salinity gradients, temperature-salinity (T-S) relationships were considered in order to study the hydrographic variations in a more concise format. The temperature versus salinity plots in Figures I-15 and I-16 are a composite of all data from all depths at all stations for the given days. Figure I-15

gives the T-S relationships for the period September 1977 through August 1978 which were described in a previous report, Hann, et al. (Feb. 1979). For the purpose of continuity these data are reviewed briefly. The relationships in September, October and November show the relatively well-mixed conditions pointed out in Figure I-2. In December 1977 through late February 1978 there is a distinct elongation along the salinity axis as a result of fresher water being present. The elongation decreases somewhat in the March 1978 data but extends again in April 1978. The sampling conducted in July 1978 (on 18, 20 and 26 July) failed to detect significantly fresher water in the study area.

Considering the T-S relationships from September 1978 through April 1979 (Fig. I-16), we see a less pronounced T-S elongation for October 1978 through March 1979 along with a more rapid change of the fresher surface water temperature with respect to the bottom saltier water. The stability of the water during this period became correspondingly weaker as the vertical salinity gradients lessened and as the temperature inversion strengthened. The T-S relationship for the April 1979 show that the T-S elongation much more pronounced; corresponding cross-shelf vertical sections indicate the expected intensification of water column stability.

In the study by Angelovic (1976), it is suggested that the principle sources of fresh water that affect the nearshore salinities are the Mississippi and Atchafalaya Rivers. An event which supports this idea can be seen in the nearshore hydrographic data collected from September through December 1977 near the Texas-Louisiana border (Anonymous, 1978). The T-S relationships from this data showed no elongation along the salinity axis up to and including 14 December. But on 16 December the elongation was present. This elongation was associated with a strong impulse of longshore

wind blowing westward. Using 50 cm/s as a mean longshore surface current toward the southwest, the Texas-Louisiana fresher water would have had a calculated arrival time in the Freeport study area on 18 or 19 December. On 18 December, the fresher water was detected in the data collected by TAMU off Freeport. The minimum salinity in December 1977 was 18.5°/$_{oo}$ for the Texas-Louisiana data but 27°/$_{oo}$ for the Freeport data. Thus it is a reasonable speculation that the fresher water detected in the present study originated near the waters of the Mississippi Delta.

There is also some geological evidence for the above mentioned idea. Considering the clay content of Texas rivers and the Mississippi River, distinct relative amounts of the clays smectite, illite, and kaolinite exist. These three minerals form the greater majority of the clays, and smectite is the major constituent for Mississippi waters (personal communication, Robert Tomkins, 1979) while it is only a minor constituent for Texas river water entering the Gulf of Mexico (Bright and Rezak, 1978). Bright and Rezak (1978) found smectite to be the dominant clay in nearly all their sediment samples along the Texas shelf, including nearshore regions. This result would indicate that the source of the fresher water is the Mississippi River.

The presence of nearshore fresher water along the Texas coast was discussed by Angelovic (1976) as well as indications of its variations and southwestward extent. The major new result of the hydrographic data set from this study is the strong pycnocline that existed between the fresher and saltier waters for a good part of the year including winter. A natural assumption was that winter turbulent mixing would result in a relatively homogeneous water column. Apparently the crowding of the fresher water next to the shore limits the surface area along which mixing can take place, and the continuous influx of fresher water can maintain the feature against any mixing that does take place.

Wind Data

Since the major hydrographic variations appear to be a result of advection, several data sets of wind velocities and wind stresses were studied. Table I-2 gives the average wind components for the time period September 1977-August 1978. The data was collected by NDBO from a location inside the study area (Fig. I-1) and average longshore (northeastward flowing wind is positive) and cross-shelf (onshore flowing wind is positive) components were calculated for periods between hydrographic surveys.

The average longshore wind shifts toward the southwest after November 1977 and stays southwestward until the middle of June 1978. The average longshore wind shifts northeastward after mid-June, reaches its maximum northeastward speeds in July 1978, and then begins a shift toward the southwest between the July and August hydrographic surveys. The average cross-shelf winds have onshore peak speeds in November 1977 and June 1978 and are offshore only during January and February 1978.

There is a clear correlation between the T-S relationships (Figs. I-15, 16) and the variations in the longshore wind speed (Table I-1). As the average longshore wind shifts from northeastward to southwestward, the T-S elongation occurs, and as the wind shifts from southwestward to northeastward the elongation disappears. As the southwestward wind weakens between the early February and March 1978 hydrographic samplings, one sees higher salinities. This data supports the speculation that the fresher water is advected into the study area from the northeast, and the advection is a result of longshore wind stress. The greater elongation seen in April 1978 is likely the result of the fact that the southwestward wind speeds are increasing during the period when the Mississippi and Atchafalaya Rivers normally have their greatest outflows (Angelovic, 1976).

The average wind data from September 1978-February 1979 are given in Table I-2. The average longshore wind is seen to remain southwestward during the fall of 1978. This is likely the reason why the fall 1978 T-S relationships were more elongated than the relationships of fall 1977. The onshore cross-shelf wind speed slackened during fall 1977, became offshore during January 1979, and then slackened again in February 1979.

If the longshore wind is the mechanism which determines whether the fresher water is present, then historical wind stress data can be used to predict the times of greatest influence of the fresher water. Monthly average longshore cross-shelf wind stresses were calculated from hourly wind data collected at Galveston, Texas, and are presented in Fig. I-17. Drag coefficients were taken from Reid and Bodine (1969). This data shows the average longshore wind stress shifting northeastward in May and southwestward in September. Thus the presence of the fresher water could be expected to occur in fall, winter and early spring. The cross-shelf wind stress is seen to be offshore during November, December, January and February.

Another historical longshore wind stress data set is shown in Fig. I-17 and is the result of the averaging of 20 years of ship observed winds near Galveston (Blaha and Sturges, 1978). The two longshore wind stress data sets are considerably different in that the data obtained from ship observations shows a maximum southwestward stress during April and September and no northeastward average wind stresses during any part of the year. Having differences between stresses calculated using coastal wind data and wind data collected offshore is not unusual (e.g. Reid et al, 1958; Mayer et al, 1979). These differences may be used to explain the zone of convergence noted by Angelovic (1976) which developed in waters of inner and middle-shelf areas. During May, June, July and August, Fig. I-17 would indicate offshore Ekman flow in the very nearshore regions and onshore Ikman flow further offshore. Thus an

offshore convergence zone would develop between the nearshore fresher waters and the offshore saltier waters. Angelovic noted that the zone was most pronounced in spring, moved northeastward during spring through early summer, and was absent from October through February. This would be the expected pattern considering Fig. I-17 and the hydrographic data collected during the summer of 1978. The historical longshore wind stress data indicates that the zone would first appear in April or May and disappear in August or September. As the nearshore fresher water is advected northeastward, it is replaced by saltier waters from the southwest, and therefore, the zone would move northeastward through the spring and summer. Also, the convergence zone would act as a mechanism to keep the fresher water in the nearshore region even while it is flowing northeastward and has an offshore Ekman component.

Thermograph Data

In-situ water temperature was measured at 15 minute intervals at the same location (Fig. I-1) as current velocity and at the same depths, i.e. approximately 3 meters below the surface and approximately 2 meters above the bottom. The sensors are General Oceanics model 3070 film recording thermographs with an accuracy of better than ±0.5°C. They have been calibrated over the range 5°-30°C against precision mercury thermometers (±0.02°C). The instruments are presently being re-calibrated to check for any significant drift, and therefore, the following discussion is based on uncalibrated data. However, the qualitative results should not be affected once the calibrations are applied.

NDBO also collected in-situ water temperature as part of their hourly meteorological data. This data has been used in the following discussion to supplement the TAMU data when there are data gaps due to instrument malfunction or loss of an instrument at sea.

Fig. I-18 shows the time series of those data sets for which both surface and bottom temperatures are available whether the data is from the TAMU thermographs, from NDBO or a combination of both. The onset of the spring/summer thermocline occurred in mid-March 1978 when heating of the surface water resulted in that water becoming warmer than the bottom water. The data from 10 June 1978 show an initial temperature difference of approximately 5°C between the surface and bottom water. On 15 June the thermocline began to disappear as the temperatures of the bottom water rose while the surface water temperature remained approximately constant. The thermocline reappeared on 24 June when the bottom water temperature fell. This same process occurred again on 5 July and 16 July 1978. The disappearence was much more abrupt for the 16 July episode, and the thermocline never reappeared to the same extent after that date.

The data point out the relatively isothermal conditions of mid-July through late October 1978. By November the bottom water was slightly warmer than the surface water, and between 9 and 15 December 1978 both surface and bottom temperatures fell by approximately 3°C. By April 1979 the bottom water was about 2°C cooler than the surface, and this difference continued through early May 1979.

Episodes of bottom water temperature variations during periods of relatively constant surface water temperatures were not uncommon (e.g. 24-28 December 1977, 14-28 June 1978, 5-8 July 1978, 16-17 July 1978, and 14-22 August 1978). Continuous data collected by NDBO from May through June 1978 also indicate that short-term temperature variations occurred at the bottom but not at the surface. These episodic changes are clearly a result of advective processes. They demonstrate that in the lower part of the water column in this area advective processes play a major role in the variation of the characteristics of the water. The data also demonstrate that the strength of the thermocline and therefore the stability of the water column can undergo significant short-term changes.

Current Data

In order to study currents, a system was placed ≈40 m from the meteorological package (Fig. I-1) and currents were measured at ≈3 m below the surface and ≈2 m above the bottom. The current meters were Environmental Devices Corporation's Type 105 tethered current meters. These meters are specifically designed for a wave zone environment and give a 30-minute average of speed and direction every half hour. The speed resolution is 2.57 cm/s^{-1} and speed accuracy is ±5.4 cm/s. Continuous surface and bottom currents were measured from 10 June-5 September 1978 and from 18 October 1978-1 March 1979. In addition, surface and bottom currents were measured within the study area from 22 December 1977-5 January 1978 (site C, Fig. I-1) and from 14-30 March 1978. (site Z, Fig.I-1)

In order to obtain a concise picture of the current regime, an event analysis of the surface currents was made. The current data, along with the corresponding wind data, were filtered to eliminate fluctuations at tidal and noise frequencies. A filter for hourly samples was devised employing the techniques advances by Groves (1955) using the ratios of tidal components for Galveston, Texas (Zetter and Hansen, 1972). The analysis consisted of breaking the December 1977, March 1978 and 30 June-5 September 1978 wind, surface current, and bottom current filtered data into 12 hour periods. The average velocity for each 12 hour period was calculated for the winds and currents, and the periods were grouped according to the following categories:

Longshore Surface Velocity u_T	$0 < u_T \leq 5$ cm/s
	$u_T > 5$ cm/s
	$-5 \leq u_T < 0$ cm/s
	$u_T < -5$ cm/s

The categories were further subdivided based on whether a thermocline existed ($|T_{surface} - T_{bottom}| > 4°C$) using the raw thermograph data. The results of the event analysis is shown in Table I-3 where

$\bar{u}$ - average longshore current (positive is northeast),

$\bar{v}$ - average cross-shelf current (positive is onshore),

$\overline{\tau_x}$ - average longshore wind stress, and

$\overline{\tau_y}$ - average cross-shelf wind stress.

The flow regimes can be put into two classes. The first class covers the December 1977, March, 30 June-16 July and 9 August-3 September 1978 periods. This class is characterized by longshore bottom and surface flows in the direction of the longshore wind stress. Also, the cross-shelf surface flow was to the right of the surface flow and the cross-shelf bottom flow was opposite to that of the surface. The cross-shelf surface flow was apparently Coriolis induced with the cross-shelf wind stress having secondary influence.

The second flow regime class covers the period from 16 July-9 August 1978. This class is characterized by longshore and cross-shelf surface flows in the direction of the longshore and cross-shelf wind stresses. The longshore bottom flow was in the direction of the longshore wind stress while the cross-shelf bottom current ran to the left of the longshore bottom flow, regardless of the direction of the cross-shelf surface flow.

Thus the picture we obtain from the first class is that of a longshore flow induced by longshore wind stress and a Coriolis induced cross-shelf surface flow with a compensating cross-shelf bottom flow. The second class again suggests a longshore flow induced by longshore wind stress but with a wind stress induced cross-shelf surface flow along with a cross-shelf bottom current running to the left of the longshore bottom current. There are a few items to note. The first is that there are several instances (e.g. 20-21 March, 20-21 July, 3-4 August, and 18-19 August 1978) that show the transition

from a positive (northeastward) longshore wind stress to a negative longshore wind stress. In each instance the bottom current shifted toward the southwest before the surface current. In the cases of a transition from southwestward to northeastward wind stress (e.g. 30 June, 23-24 July 1978), the longshore currents at the surface shifted first. This implies a longshore surface elevation gradient toward the northeast.

It should also be noted that for both classes of flow regimes the cross-shelf bottom current tended to flow to the left of the longshore bottom current. Thus the cross-shelf bottom flow for both regimes could be explained in terms of the deflection of the longshore current toward the left as it nears the frictional influence of the bottom.

The principle difference between the two flow regimes appears to be the influence of the cross-shelf wind stress. Hydrographic data indicate that the first flow regime was associated with the presence of the fresher water and the second flow regime was associated with the absence of the fresher water. When the fresher water was present, the cross-shelf surface currents apparently were not influence by the cross-shelf wind stress but were a result of the Coriolis effect on the longshore current. When the fresher water was absent, the cross-shelf currents responded to the cross-shelf wind stress. This can be explained by the shallowness of the study area and the limited offshore extent of the fresher water (10-30 km). Wind-induced accelerations will be limited before the fresher water is downwelled (either at the shore or at the offshore boundary of the fresher water). The downwelled water is affected by bottom friction due to the shallowness of the water, and the cross-shelf wind-induced accelerations are further weakened. Thus the cross-shelf wind-induced accelerations would be small and could be overcome by Coriolis induced accelerations on the longshore current. It is quite likely that beyond the fresher water

the cross-shelf wind stresses do result in cross-shelf currents since the fetch is not as limited. This is seen to occur in the second flow regime, and these onshore cross-shelf currents beyond 30 km, which are onshore for most of the year (Fig. I-6), could act as another mechanism for containing fresher water close to shore.

The flow regime in the presence of lighter water overlying heavier water is as predicted by the theoretical work of Csanady (1977). His work considered a frictionless case and showed that a longshore wind stress initiated a surface flow in the same direction of the wind stress with a Coriolis-induced cross-shelf surface flow throughout the layer of lighter water. The longshore accelerations change the inclination of the interface between the two water types because the momentum balance in the cross-shelf direction is always geostrophic. This change induces a cross-shelf flow through the bottom layer which compensates the flow in the top layer. Longshore currents in the bottom layer are thus generated in the direction of the wind stress through the action of the Coriolis force on the cross-shelf current.

The results shown in Table I-5 indicate how well the cross-shelf geostrophic assumption holds for the periods when hydrographic and current meter data were collected up to 1 September 1978. Hydrographic data from stations near the current meter string were used to calculate the geostrophic longshore surface current, and the current meter speeds are estimates of the average speed from the filtered current meter data. The greatest differences between the two speed data sets occur on 20, 21 and 22 June 1978. The differences increase with each day with the geostrophic data indicating an increasing flow toward the southwest while the current meter data indicating a decreasing flow toward the southwest. On 23 June

1978, both surface and bottom current meters show a change in the signs of the longshore and cross-shelf currents (going from a flow regime with fresher water present toward the southwest to a flow regime toward the northeast). Thus the discrepancies between the June estimates and measurements of longshore currents are most likely the result of the accelerations that must occur as the flow regime goes through a change in longshore direction. If the June data are not considered, the average percent error from Table I-5 is 12.4%, indicating reasonable agreement.

Bottom Current Speeds Versus Wind Stresses

Since the longshore currents appear to be correlated with the longshore wind stress, plots were made of corresponding 12 hour average values of longshore bottom current speed and wind stress for various periods. For each period, the point for each pair of 12 hour averages was sequencially numbered (i.e. point 1 represents the first pair of 12 hour averages, point 2 represents the next pair of 12 hour averages, etc.). The objective of creating these plots is to investigate the relationship between the longshore wind stress and the corresponding longshore bottom current in order to determine whether an emperical relationship could be developed between the two data sets.

Considering the December 1977 data (Fig. I-19), we see a general pattern (shown by dashed lines) which suggests an elliptical relationship with an indentation in it. The ellipse is a result of the phase lag between a change in the wind stress and a change in the bottom current. The deviation from an elliptical pattern (points 7, 8, 9, and 10) is a result of a temporary slackening in the wind stress. This same type of pattern occurs in the 30 June-16 July 1978 data (Fig. I-20). The top part of an ellipse can be seen in the relationships of points 1 through 7, and the right hand side of it can be seen in the relationships of points 31 through 35. It is interesting to note that for five days (points 20-29) the bottom currents ran counter to the wind stress. This apparently was due to the slackening of the wind stress to values less than 0.1 dynes/cm^{-2} for an extended period and to the longshore surface elevation gradient. For the data of 29 July-9 August 1978 (Fig. I-21), the bottom and left hand side of the elliptical pattern are outlined by points 7-23. As for the March 1978 data (Fig. I-22), only parts of elliptical patterns can be made out (e.g. points 6-15).

The results of Figs. I-19 through I-22 point out that the bottom longshore current is related to some function of time integrated wind stress. The size and orientation of the elliptical pattern is dependent on the previous history of wind stress and the response of the longshore currents to that wind stress. The December 1977 data (Fig. I-19) shows a large well-developed pattern due to the strong and fairly consistently varying longshore wind stress. The patterns that occur in summer (Figs. I-20 and I-21) are smaller and show fluctuations during periods when the longshore surface elevation gradient can overcome an opposing longshore wind stress.

Thus the relationships between the longshore components of wind stress and bottom currents are at best a family of ellipses with varying orientations with respect to the current speed axis and varying eccentricities. Although this situation makes it most difficult to develop a set empirical relationship, it does lend itself to examination theoretically.

Theoretical Considerations

To obtain a greater insight into the physical processes between winds and current response at various frequencies, a theoretical model was developed for a two layer, nearshore coastal sea. Consider a semi-infinite coastal sea bounded by a straight coastline coincident with the x-axis and with the y-axis being negative out to sea. The water column consists of a slightly lighter top layer of equilibrium depth h_1 and density ρ_1. Below this layer is denser water of equilibrium depth h_2 and density ρ_2. The term $\varepsilon = (\rho_2 - \rho_1)/\rho_2$ is small, of order 10^{-3}.

The following definition of variables will be used:

η_1: Deviation of the water surface from its undisturbed position of $z = 0$.

η_2: Deviation of the interface surface from its undisturbed position of $z = -h_1$.

u: The vertically averaged longshore current. The subscript 1 refers to the surface layer and 2 to the bottom layer.

v: The vertically averaged cross-shelf current. Again the subscripts 1 and 2 will denote the surface and bottom layers, respectively.

τ_x, τ_y: The longshore and cross-shelf components of the wind stress, respectively.

g: acceleration due to gravity.
t: time
f: the Coriolis parameter

For the surface layer, the vertically integrated equations of motion are:

$$\frac{\partial u_1}{\partial t} - fv_1 + g\frac{\partial \eta_1}{\partial x} = \frac{\tau_x}{h_1}$$

$$\frac{\partial v_1}{\partial t} + fu_1 + g\frac{\partial \eta_1}{\partial y} = \frac{\tau_y}{h_1} \qquad (1)$$

$$\frac{\partial(\eta_1-\eta_2)}{\partial t} + \frac{\partial(h_1u_1)}{\partial x} + \frac{\partial(h_1v_1)}{\partial y} = 0$$

For the underlying layer, we have:

$$\frac{\partial u_2}{\partial t} - fv_2 + g\frac{\partial}{\partial x}\{\eta_1 - \varepsilon(\eta_1 - \eta_2)\} = 0$$

$$\frac{\partial v_2}{\partial t} + fu_2 + g\frac{\partial}{\partial y}\{\eta_1 - \varepsilon(\eta_1 - \eta_2)\} = 0 \qquad (2)$$

$$\frac{\partial \eta_2}{\partial t} + \frac{\partial(h_2u_2)}{\partial x} + \frac{\partial(h_2v_2)}{\partial y} = 0$$

We multiply the first two equations in (1) by h_1 and the first two equations in (2) by αh_2 and add the equations together. The results are:

$$\frac{\partial}{\partial t}\{h_1u_1 + h_2u_2\alpha\} + f\{h_1v_1 + h_2v_2\alpha\} + g\frac{\partial}{\partial x}\{h_1\eta_1 + h_2\alpha(\eta_1 - \varepsilon(\eta_1 - \eta_2))\} = \tau_x \qquad (3)$$

$$\frac{\partial}{\partial t}\{h_1v_1 + h_2v_2\alpha\} + f\{h_1u_1 + h_2u_2\alpha\} + g\frac{\partial}{\partial y}\{h_1\eta_1 + h_2\alpha(\eta_1 - \varepsilon(\eta_1 - \eta_2))\} = \tau_y$$

We multiply the last equation in (2) by α and add to the last equation in (1). This result is:

$$\frac{\partial}{\partial}\{\eta_1 - \eta_2 + \alpha\eta_2\} + \frac{\partial(h_1u_1 + h_2u_2\alpha)}{\partial x} + \frac{\partial(h_1v_1 + h_2v_2\alpha)}{\partial y} = 0 \qquad (4)$$

We can now define some new variables. Let:

$$Q_x = h_1u_1 + h_2\alpha u_2,$$

$$Q_y = h_1v_1 + h_2\alpha v_2.$$

We now want to get elevation anomolies to be the same in equations (3) and (4), so let

$$h_1\eta_1 + h_2\alpha(\eta_1 - \varepsilon(\eta_1 - \eta_2)) = \Gamma(\eta_1 - \eta_2 + \alpha\eta_2) \tag{5}$$

where Γ is a constant with dimensions of length. Now let $\phi = \eta_1 - \eta_2 + \alpha\eta_2$. We can rewrite (3) and (4) as

$$\begin{aligned} &\frac{\partial Q_x}{\partial t} - fQ_y + g\Gamma\frac{\partial \phi}{\partial x} = \tau \\ &\frac{\partial Q_y}{\partial t} + fQ_x + g\Gamma\frac{\partial \phi}{\partial y} = \tau \\ &\frac{\partial \phi}{\partial t} + \frac{\partial Qx}{\partial x} + \frac{\partial Qy}{\partial y} = 0 \end{aligned} \tag{6}$$

Let's consider equation (5) in more detail. If $\eta_1 - \eta_2 = 0$, then we have

$$h_1\eta_1 + h_2\alpha\eta_1 = \Gamma\alpha\eta_2$$

or

$$h_1 + h_2\alpha = \Gamma\alpha. \tag{7}$$

If $\eta_1 = 0$, then we have

$$\alpha h_2\varepsilon\eta_2 = \Gamma(-\eta_2 + \alpha\eta_2)$$

or

$$\alpha\varepsilon h_2 = \Gamma(\alpha - 1) \tag{8}$$

Eliminating Γ gives a quadratic equation for α with the roots

$$\alpha = \frac{(h_2 - h_2) \pm \{(h_1 + h_2)^2 - 4h_1h_2\varepsilon\}^{\frac{1}{2}}}{2h_2(1-\varepsilon)}$$

Since $\varepsilon << 1$ for oceanic conditions, the approximate roots are

$$\alpha_1 = \frac{1-\varepsilon\dfrac{h_1}{(h_1+h_2)}}{1-\varepsilon} + O(\varepsilon^2)$$

$$\alpha_2 = \frac{-\dfrac{h_1}{h_2} + \varepsilon\dfrac{h_1}{(h_1+h_2)}}{1-\varepsilon} + O(\varepsilon^2) \qquad (9)$$

Thus the corresponding Γ are

[from (7)]

$$\Gamma_1 = \frac{h_1}{(1-\varepsilon\dfrac{h_2}{h_1+h_2})} + h_2 + O(\varepsilon) \qquad \simeq h_1 + h_2$$

[from (8)]

$$\Gamma_2 = \frac{h_2\varepsilon}{1-\dfrac{1}{-\dfrac{h_1}{h_2}+\varepsilon\dfrac{h_1}{h_1+h_2}}} \qquad \simeq \frac{h_1h_2\varepsilon}{h_1+h_2} \quad \text{since } \varepsilon << 1$$

Therefore, our corresponding variables are

$$Q_{x_1} = h_1u_1 + h_2u_2$$

$$Q_{y_1} = h_1v_1 + h_2v_2$$

$$Q_{x_2} = h_1(u_1 - u_2) \qquad (10)$$

$$Q_{y_2} = h_1(v_1 - v_2)$$

$$\phi_1 = \eta_1$$

$$\phi_2 = \eta_1 - \eta_2\{1+\frac{h_1}{h_2}\} \simeq -\eta_2\frac{(h_1+h_2)}{h_2} \qquad (11)$$

The approximation for ϕ_2 is made since the variations at an interface are normally large with respect to the variations at the surface.

We wish to work with equations in (16). For time periodic forcing. we have

$$\tau_x = \tau_x^\circ e^{i\omega t}$$
$$\tau_y = \tau_y^\circ e^{i\omega t}$$

Assume that the changes of variables in the longshore direction are negligible. This gives

$$\frac{\partial Q_x}{\partial t} - fQ_y = \tau_x$$
$$\frac{\partial Q_y}{\partial t} + fQ_x + g\Gamma\frac{\partial \phi}{\partial y} = \tau_y \qquad (12)$$
$$\frac{\partial \phi}{\partial t} + \frac{\partial Q_y}{\partial y} = 0$$

Also assume that the response is of the character

$$\begin{bmatrix} Q_x \\ Q_y \\ \phi \end{bmatrix} = \begin{bmatrix} Q_x^\circ e^{i\omega t} \\ Q_y^\circ e^{i\omega t} \\ \phi^\circ e^{i\omega t} \end{bmatrix}$$

Thus equation (12) reduces to

$$i\omega Q_x^\circ - fQ_y^\circ = \tau_x^\circ$$
$$i\omega Q_y^\circ + fQ_x^\circ + g\Gamma\frac{\partial \phi}{\partial y} = \tau_y^\circ \qquad (13)$$
$$i\omega\phi^\circ + \frac{\partial Q_y^\circ}{\partial y} = 0$$

From the last equation in (13) we have

$$\phi^\circ = -\frac{1}{i\omega}\frac{\partial Q_y^\circ}{\partial y}$$

From the first equation in (13) we have

$$Q_x^\circ = \frac{\tau_x^\circ + fQ_y^\circ}{i\omega} \qquad (14)$$

Putting these relationships into the second equation in (13) and using $C^2 = g\Gamma$, we obtain

$$C^2\frac{\partial Q_y^{\circ 2}}{\partial y^2} + Q_y^\circ(\omega^2 - f^2) = \{f\tau_x^\circ - i\omega\tau_y^\circ\} \qquad (15)$$

For the homogenous solution of (15) try $Q_y^\circ = Ae^{my}$. This would give

$$C^2m^2 - f^2 + \omega^2 = 0$$

or

$$m = \pm\{\frac{f^2 - \omega^2}{C^2}\}^{\frac{1}{2}}$$

We will use the positive root in order that Q_y° becomes constant as $y \to -\infty$. For the particular solution, let τ_y and τ_x be independent of y. The particular solution to (15) would be

$$Q_y^\circ = \frac{i\omega\tau_y^\circ - f\tau_x^\circ}{(f^2 - \omega^2)}$$

so that the complete solution would be

$$Q_y^\circ = Ae^{my} + \frac{i\omega\tau_y^\circ - f\tau_x^\circ}{(f^2 - \omega^2)}$$

At y = 0 (the shore) we want $Q_y^\circ = 0$, so

$$Q_y^\circ = \frac{i\omega\tau_y^\circ - f\tau_x^\circ}{(f^2 - \omega^2)}\{1 - e^{my}\} \tag{16}$$

$$\text{where} \quad m = \{\frac{f^2 - \omega^2}{C^2}\}^{\frac{1}{2}}$$

We can now go back to equation (14) and solve for Q_x°:

$$Q_x^\circ = \frac{1}{i\omega}\{\tau_x^\circ + f\frac{i\omega\tau_y^\circ - f\tau_x^\circ}{(f^2 - \omega^2)}\{1 - e^{my}\}\} \tag{17}$$

From the relationship $\phi^\circ = -\frac{1}{i\omega}\frac{\partial Q_y^\circ}{\partial y}$, we have

$$\phi^\circ = \frac{(i\omega\tau_y^\circ - f\tau_x^\circ)m}{i\omega(f^2 - \omega^2)}e^{my}$$

Using the relationships in (16) and (17) we can now solve for $\eta_1, \eta_2, u_1, v_1, u_2, v_2$. If $\tau_y = 0$, then

$$Q_y^\circ = \frac{f\tau_x^\circ}{(f^2 - \omega^2)}\{e^{my} - 1\}$$

$$Q_x^\circ = \frac{i\tau_x^\circ}{\omega}\left\{\frac{f^2(1-e^{my})}{(f^2-\omega^2)} - 1\right\}$$

$$\phi^\circ = \frac{if\tau_x^\circ m}{\omega(f^2-\omega^2)}\, e^{my} \qquad (18)$$

If $\tau_x = 0$, then

$$Q_y^\circ = \frac{i\omega\tau_y^\circ}{(f^2-\omega^2)}\left\{1 - e^{my}\right\}$$

$$Q_x^\circ = \frac{f\tau_y^\circ}{(f^2-\omega^2)}\left\{1 - e^{my}\right\} \qquad (19)$$

$$\phi^\circ = \frac{\tau_y^\circ m}{(f^2-\omega^2)}\, e^{my}$$

Thus we have for sinusoidally varying longshore wind stress

$$\eta_1 = \frac{-f\tau_x^\circ \sin\omega t}{\omega(f^2-\omega^2)}\, m_1 e^{m_1 y}$$

$$u_1 = \frac{f^2\tau_x^\circ \sin\omega t}{\omega(h_1+h_2)(f^2-\omega^2)}\left\{e^{m_1 y} + \frac{h_2}{h_1}e^{m_2 y} - \frac{\omega^2(h_1+h_2)}{h_1 f^2}\right\}$$

$$v_1 = \frac{f\tau_x^\circ \cos\omega t}{h_1(f^2-\omega^2)(h_1+h_2)}\left\{h_1(e^{m_1 y}-1) + h_2(e^{m_2 y}-1)\right\}$$

$$\eta_2 = \frac{fh_2\tau_x^\circ \sin\omega t}{(h_1+h_2)\omega(f^2-\omega^2)}\, m_2 e^{m_2 y}$$

$$u_1 = -\frac{f^2\tau_x^\circ \sin\omega t}{\omega(h_1+h_2)(f^2-\omega^2)}\left\{e^{m_2 y} - e^{m_1 y}\right\}$$

$$v_1 = \frac{f\tau_x^\circ \cos\omega t}{(h_1+h_2)(f^2-\omega^2)}\left\{e^{m_1 y} - e^{m_2 y}\right\} \qquad (20)$$

For a sinusoidally varying cross-shelf wind stress, we have

$$\eta_2 = \frac{\tau_y^\circ \cos \omega t}{(f^2 - \omega^2)} m_1 e^{m_1 y}$$

$$u_1 = \frac{f\tau_y^\circ \cos \omega t}{h_1(h_1 + h_2)(f^2 - \omega^2)} \{h_1(1 - e^{m_1 y}) + h_2(1 - e^{m_2 y})\}$$

$$v_1 = \frac{\omega\tau_y^\circ \sin \omega t}{h(h_1 + h_2)(f^2 - \omega^2)} \{h_1(e^{m_1 y} - 1) + h_2(e^{m_2 y} - 1)\}$$

$$\eta_2 = -\frac{fh_2\tau_y^\circ \cos \omega t}{(h_1 + h_2)\omega(f^2 - \omega^2)} m_2 e^{m_2 y}$$

$$u_2 = \frac{f\tau_y^\circ \cos \omega t}{(h_1 + h_2)(f^2 - \omega^2)} \{e^{m_2 y} - e^{m_1 y}\} \qquad (21)$$

$$v_2 = \frac{\omega\tau_y^\circ \sin \omega t}{(h_1 + h_2)(f^2 - \omega^2)} \{e^{m_1 y} - e^{m_2 y}\}$$

We will let $R_1 = \frac{1}{m_2}$ and $R_2 = \frac{1}{m_2}$ so that

$$R_1 = \left\{\frac{g(h_1 + h_2)}{f^2 - \omega^2}\right\}^{\frac{1}{2}}, \quad R_2 = \left\{\frac{gh_1h_2\varepsilon}{(f^2 - \omega^2)(h_1 + h_2)}\right\}^{\frac{1}{2}}$$

Thus R_1 is the barotropic radius of deformation, and R_2 is the much smaller baroclinic radius of deformation.

Suppose we have the longshore wind stress $\tau_x^\circ \cos wt$. For nearshore areas where $y << R_2$ (and thus $y << R_1$ also), we have

$$\eta_1 = -\frac{f\tau_x^\circ \sin \omega t}{\omega(f^2 - \omega^2)R_1}$$

$$u_1 = \frac{\tau_x^\circ \sin \omega t}{h_1\omega}$$

$$v_1 = 0 \qquad (22)$$

$$\eta_2 = \frac{fh_2\tau_x^\circ \sin \omega t}{\omega(h_1 + h_2)(f^2 - \omega^2)R_2}$$

$$u_2 = 0$$

$$v_2 = 0$$

Hence we see that the wind stress is distributed over the surface layer only and generates a longshore current that lags the wind stress by 90° and reduced by the factor of ω^{-1}. The surface elevation η_1 varies opposite to u_1, as expected, while η_2 varies directly with u_1.

In the same region but with cross-shelf wind stress $\tau_y^\circ \cos \omega t$, we have

$$\eta_1 = \frac{\tau_y^\circ \cos \omega t}{(f^2 - \omega^2) R_1}$$

$$\begin{aligned} u_1 &= 0 \\ v_2 &= 0 \\ \eta_2 &= -\frac{f h_2 \tau_y^\circ \cos \omega t}{\omega (h_1 + h_2)(f^2 - \omega^2) R_2} \\ u_2 &= 0 \\ v_2 &= 0 \end{aligned} \tag{23}$$

Thus the cross-shelf wind stress does not generate any currents in this region since we are not allowing any longshore variations. The wind stress results in the surface elevation varying directly with the stress and the interface η_2 varying opposite to η_1.

For the region such that $R_2 << y << R_1$, we have for a longshore wind stress

$$\eta_1 = \frac{-f \tau_x^\circ \sin \omega t}{\omega (f^2 - \omega^2) R_1}$$

$$u_1 = \frac{\tau_x^\circ \sin \omega t}{h_1 \omega (f^2 - \omega^2)(h_1 + h_2)} \{h_1 f^2 - \omega^2 (h_1 + h_2)\}$$

$$v_1 = \frac{-f h_2 \tau_x^\circ \cos \omega t}{(f^2 - \omega^2)(h_1 + h_2) h_1}$$

$$\begin{aligned} \eta_1 &= 0 \\ u_2 &= \frac{f^2 \tau_x^\circ \sin \omega t}{\omega (h_1 + h_2)(f^2 - \omega^2)} \\ v_2 &= \frac{f \tau_x^\circ \cos \omega t}{(h_1 + h_2)(f^2 - \omega^2)} \end{aligned} \tag{24}$$

We see here that u_1 and u_2 lag the wind stress by 90° for the normal sub-inertial condition of $h_1 f^2 > \omega^2 (h_1+h_2)$. The elevation of the pycnocline is negligible and the cross-shelf transport in the surface layer it totally compensated by that in the bottom layer. The cross-shelf surface current varies directly with the wind stress but to the right of wind stress direction.

For a cross-shelf wind stress in the same region, we have

$$\eta_1 = \frac{\tau_y^\circ \cos \omega t}{(f^2 - \omega^2) R_1}$$

$$u_1 = \frac{h_2 f \tau_y^\circ \cos \omega t}{(h_1 + h_2)(f^2 - \omega^2) h_1}$$

$$v_1 = -\frac{h_2 \omega \tau_y^\circ \sin \omega t}{h_1 (h_1 + h_2)(f^2 - \omega^2)}$$

$$\eta_2 = 0$$

$$u_2 = -\frac{f \tau_y^\circ \cos \omega t}{(h_1 + h_2)(f^2 - \omega^2)}$$

$$v_2 = \frac{\omega \tau_y^\circ \sin \omega t}{(h_1 + h_2)(f^2 - \omega^2)}$$

Thus the longshore surface transport generated is in phase and to the right of the wind stress and is exactly compensated by longshore transport in the bottom layer. The cross-shelf surface and bottom transports compensate one another, and it is interesting to note that the surface cross-shelf current lags η_1 by 270°.

For the region $y \ll R_1$, we have for the longshore wind stress case

$$\eta_1 = 0$$

$$u_1 = -\frac{\omega\tau^{\circ}_x \sin \omega t}{h_1(f^2 - \omega^2)}$$

$$v_1 = -\frac{f\tau^{\circ}_x \cos \omega t}{h_1(f^2 - \omega^2)}$$

$$\eta_2 = 0$$

$$u_2 = 0$$

$$v_2 = 0$$

Thus the wind stress effects the surface layer only by generating cross-shelf surface currents to the right and in phase with the longshore wind stress and longshore surface currents that lag the longshore wind by 270°.

For cross-shelf wind stress in the above region,

$$\eta_1 = 0$$

$$u_1 = \frac{f\tau^{\circ}_y \cos \omega t}{h_1(f^2 - \omega^2)}$$

$$v_1 = -\frac{\omega\tau^{\circ}_y \sin \omega t}{h_1(f^2 - \omega^2)}$$

$$\eta_2 = 0$$

$$u_2 = 0$$

$$v_2 = 0,$$

and the results are correspondingly the same as for the longshore wind stress.

The overall results of all of the above equations are as follows:

1. For sinusoidally varying longshore wind stress, no motion is generated in the bottom layer except in the region such that

$R_2 << y << R_1$. As long as $y << R_1$, the longshore currents lag the longshore wind stress by 90°. For $y << R_1$, the longshore surface current flows opposite to that of the regions where $y << R_2$ and $R_2 << y << R_1$. The variation of cross-shelf surface currents is 180° out of phase with the wind stress.

2. For sinusoidally varying cross-shelf wind stress, no currents are generated if $y << R_2$, and no bottom currents are generated if $y << R_1$. The surface longshore currents are in phase with the wind stress while the bottom longshore current flows opposite to the surface longshore current.
3. The v component of speed precedes the u component by 90° in all cases except for the surface components for longshore stress in the region $R_2 << y << R_1$. There the u surface component precedes the v surface component by 90°.

The set of equations derived in this manner are in a generalized form for frequency and have a singularity at $\omega = f$. On taking the limit as $\omega \to 0$, the equations in (20) and (21) reduce to those of Csanady (1977). If we consider the phase relationships between the wind stresses and the corresponding u_1, v_1, u_2, and v_2 in the intermediate region ($R_2 << y << R_1$), then we have the following relationships,

For longshore stress τ_x,

τ_x precedes u_1 by 90°,

τ_x precedes v_1 by 180°,

τ_x precedes u_2 by 90°, and

τ_x and v_2 are in phase.

For cross-shelf stress τ_y,

τ_y and u_1 are in phase,

τ_y precedes v_1 by 270°,

τ_y precedes u_2 by 180°, and

τ_y precedes v_2 by 90°.

As for the variances, we have

For longshore stress,

$\text{Var}[u_1] > \text{Var}[v_1]$,

$\text{Var}[u_2] > \text{Var}[v_2]$, and

$\text{Var}[u_2] > \text{Var}[u_1]$.

For cross-shelf stress,

$\text{Var}[u_1] > \text{Var}[v_1]$,

$\text{Var}[u_2] > \text{Var}[v_2]$, and

$\text{Var}[u_1] \begin{cases} > \text{Var}[u_2] \text{ if } h_2 > h_1 \\ < \text{Var}[u_2] \text{ if } h_2 < h_1 \end{cases}$

For $\tau_x \approx \tau_y$,

$\text{Var}[u_1]_{\tau_x} > \text{Var}[u_1]_{\tau_y}$

$\text{Var}[v_1]_{\tau_x} > \text{Var}[v_1]_{\tau_y}$

$\text{Var}[v_2]_{\tau_x} > \text{Var}[u_2]_{\tau_y}$, and

$\text{Var}[v_2]_{\tau_x} > \text{Var}[v_2]_{\tau_y}$

where the variances of a speed component as a result of the longhsore and cross-shelf stresses are $\text{Var}[\ ]_{\tau_x}$ and $\text{Var}[\ ]_{\tau_y}$, respectively. The amount that one variance is greater than another decreases as $\omega \to f$ except for the cases where $\text{Var}[u_2] > \text{Var}[u_1]$ (decreases as $\omega \to 0$) and $\text{Var}[u_1] \gtrless \text{Var}[u_2]$.

The above relationships for phases and variances may be used while considering power, coherence, and phase spectra from actual wind stress and current data.

Power, Coherence, and Phase Spectra

The power, coherence, and phase spectra were considered for sub-inertial frequencies for filtered wind stress and surface and bottom currents. A little more than 60 days worth of data were used for the periods June 30 - September 5, 1978 (summer data), October 18 - December 31, 1978 (fall data), and November 30, 1978 - February 5, 1979 (winter data). This power spectra for these data sets are shown in Figs. I-23, I-24 and I-25. The summer data shows that the power of the longshore wind stress was approximately equal to that of the cross-shelf wind stress at all frequencies (Fig. I-23). The fall data shows a significant increase in power at all frequencies for both the longshore and cross-shelf stresses with the cross-shelf powers becoming greater than the corresponding longshore powers. The longshore and cross-shelf stresses continued their increases in power as shown by the winter data spectra. During winter, the cross-shelf power was greater than the longshore power except for frequencies greater than 0.55 cycles per day (cpd). Above 0.55 cpd, the longshore and cross-shelf stresses had approximately the same power with the winter cross-shelf power being approximately equal to that of the fall cross-shelf power.

The power spectra of the surface and bottom current components for the three data sets (Figs. I-24 and I-25 are similar in many respects. In general, the power of the longshore components was greater than the power of the corresponding cross-shelf components for all three data sets. Also, the power of the longshore components (surface and bottom) tended to increase from summer to fall and from fall to winter except

at the highest and lowest frequencies. The variation of the powers of the cross-shelf components were more limited. In all, the power spectra indicate that increases in cross-shelf and longshore wind stress power tend to increase the power of the longshore surface and bottom currents.

Since the power spectra is a measure of the amount of variance that occurs per frequency, we may consider the relationships considered at the end of the last section. We can consider the summer data as a situation in which $\tau^{\circ}_x \simeq \tau^{\circ}_y$. Our previous discussion showed that the variance of the longshore stress-induced u_1, v_1, u_2, and v_2 should dominate the cross-shelf stress-induced u_1, v_1, u_2, and v_2 respectively. For longshore stressing, we had:

$$\begin{aligned} &\mathrm{Var}[u_1] > \mathrm{Var}[v_1], \\ &\mathrm{Var}[u_2] > \mathrm{Var}[v_2], \text{ and} \\ &\mathrm{Var}[u_2] > \mathrm{Var}[u_1] \end{aligned}$$

where the amount of the inequality decreased as $w \to f$ for the first two expressions but decreases as $\omega \to 0$ for the third expression. The summer power spectra of Figs. I-24 and I-25 support the first two inequalities but also indicate that:

$$\mathrm{Var}[u_1] > \mathrm{Var}[u_2].$$

This could be explained by recalling the facts that u_1 and u_2 (theoretical) are vertically averaged longshore currents whereas u_1 and u_2 (measured) are speeds at 2m below the surface (where speeds tend to be the highest) and 2m above the bottom. The measured u_2 would be effected by the frictional influence of the nearby bottom, and this could explain the above discrepency between the variance results of a frictionless model and actual data.

The winter stress spectra indicate the possibility of using that data set as one in which cross-shelf stress induced currents dominates. But consideration must be given to the theoretical ratios as, for instance, $\mathrm{Var}[u_2]_{LS}/\mathrm{Var}[u_2]_{CS}$. Using the previously developed relations for the intermediate region of $R_2 \ll y \ll R_1$, we have

$$\frac{\mathrm{Var}[u_2]_{LS}}{\mathrm{Var}[u_2]_{CS}} = \frac{f^2\tau_x^{o2}}{\omega^2\tau_y^{o2}} .$$

Thus the only time when the cross-shelf stress induced currents dominate (i.e. the value of the ratio is less than one) is when $f^2\tau_x^{o2} < \omega^2\tau_y^{o2}$. Using the winter stress power spectra, the value of τ_x^{o2}/τ_y^{o2} varies from approximately 0.25 to 0.5 indicating that cross-shelf induced currents dominate for periods less than 1.63 to 1.45 days. Thus for the subinertial frequencies, the longshore stress induced currents would still dominate. The results of the winter data show the power of the two longshore components being greater than that of the power of the two cross-shelf components. The data also shows that the power of the surface longshore component was greater than that of the bottom longshore component, but again this could have been the result of the frictional influence of the bottom.

The coherence and phase spectra between wind stress and currents for the summer data is shown in Figs. I-26 and I-27. Considering the wind stress and surface current data (Fig. I-26), we see substantial coherence between the longshore wind stress and the longshore current with an average phase of -70°, in good agreement with the theoretical shift of -90°. Most of the remainder of the coherences were below the 90% confidence limit.

Considering the summer wind stress and bottom current coherence and phase spectra (Fig. I-27), we find coherences between the longshore stress and longshore bottom currents that tend to be greater than the coherences between the longshore stress and longshore surface currents. The average

phase shift for these coherences was -67°, again very close to the theoretical shift of -90°.

The coherences for the fall data set show no pattern of relationships between wind stresses and surface currents (Fig. I-28). The longshore current was relatively coherent with both the longshore and cross-shelf wind stresses at a frequency of 0.64 cpd with a -22° phase shift for the longshore stress (theoretically, it should be -90°) and a 15° phase shift for the cross-shelf stress (close to the 0° theoretical shift). As for the coherence between the fall wind stresses and bottom currents (Fig. I-29), the only significant coherences occurred between longshore wind stress and longshore current at low frequencies. The average phase shift of -14° is not in agreement with the theoretical shift of -90°.

The winter set of coherences (Figs. I-30 and I-31) are from a period when cross-shelf wind stress power dominated over longshore wind stress power at the higher frequencies. The results show strong coherence between the cross-shelf wind stress and surface and bottom longshore and cross-shelf currents at most frequencies. This offers a good opportunity to compare a full set of theoretical phase shifts with the average phase shifts of real data (computed using only those phase shifts of statistically significant coherences). Table I-5 shows this comparison. We see that the maximum difference is 116° and that the actual u_1 and u_2 are not 180° out of phase. The recorded longshore surface and bottom currents were close to being in phase with one another and had an average phase shift of about -270° with respect to the cross-shelf wind stress. The model's inability to predict these phase relationships may be due to the fact that bottom friction is not considered and, theoretically, the current regime should be dominated by the longshore wind stress.

The coherence between wind speeds and currents were studied by Huyer and Pattullo (1972) using data collected off the Oregon shelf during the summer of 1969. The current meter data was collected at 40m below the surface in 100m of water. The power spectra showed that most of the wind energy was in the longshore component for low frequencies (< 0.6 cpd) but that the most powerful current component shifted from longshore for frequencies less than 0.3 cpd to cross-shelf for frequencies greater than 0.3 but less than 0.6 cpd. Huyer and Pattullo's coherences were similar to those of the summer data of the present study in that the only significant coherences occurred between the longshore wind and longshore current with a phase shift of between 0^{o} to -30^{o}.

Summary

Variations in the hydrography of the inner coastal zone near Freeport, Texas, are primarily a result of salinity variations which in turn are a result of advection into the area of relatively fresh water. The fresher water is in the form of a surface core of water running parallel to the coast, and its presence results in a relatively stable water column throughout much of the year. Although shallow water frontal zones due to salinity differences in winter have been reported (Nowlin and Parker, 1974; Angelovic, 1976), the magnitude of these differences and the form of the front have not been previously recorded and documented because most hydrographic surveys along the upper Texas Coast have had very few stations within 35 km of the coast.

The salinity stratification, seen in cross-shelf vertical sections, temperature vs. salinity plots and indirectly in density and Richardson number plots, is strongest during the winter and spring months (January through April), weak during the summer and non-existent during the late fall. Temperature effects are less pronounced. The average temperature of the water column varies from a low of about 9.5°C in February to a high of about 30°C in the summer months. The water column is relatively isothermal from about August through February. The spring/summer thermocline begins in about mid-March and reaches a maximum top-to-bottom difference of about 5°C. The net effect of temperature and salinity on stratification at the diffuser site, in terms of the Richardson number, is that the surface layer is generally stratified ($Ri>10$) in the winter and spring months and transitional ($0.1<Ri<10$) in the summer and fall months; the bottom layer is transitional year-round with occasional well-mixed ($Ri<0.1$) conditions in the fall and winter.

The advection of relatively fresh water into the area is correlated with the mean longshore wind: as the mean longshore wind shifts from northeastward to southwestward the salinity stratification, as shown by temperature vs.

salinity plots, increases. The evidence indicates that the source of the fresher water is to the northeast of the study area, possibly the Atchafalaya and/or Mississippi rivers.

The currents in the area are a function of both the wind stress and the presence of the fresher water. An event analysis of the current meter data indicates the existence of two flow regimes. In both regimes the longshore surface and bottom flows are in the direction of the longshore wind stress, and the cross-shelf bottom current is to the left of the longshore bottom current. In the first regime, which is associated with the presence of the fresher water, the cross-shelf surface current flows to the right of the longshore surface current and is independent of the cross-shelf wind stress. The cross-shelf surface current is apparently Coriolis-induced. In the second class, i.e. no stratification, the cross-shelf current is related to the cross-shelf wind stress.

The magnitude of the longshore bottom current as a function of longshore wind stress was investigated. The results indicate that the bottom longshore current speed is a function of the time-integrated wind stress, but an impirical relation was not found.

A theoretical model for a two-layer, frictionless nearshore sea was developed. The theoretical relationships for phases and variances are compared with actual power, coherence and phase spectra of wind stress and current data.

REFERENCES

Angelovic, J.W., 1976. Environmental studies of the south Texas outer continental shelf, 1975. Volume II, physical oceanography. NMFS, Gulf Fisheries Center, Galveston, Texas.

Anonymous, 1977-78. Climatological Data, Texas. NOAA Environmental Data Service, National Climatic Center, Asheville, N.C.

Blaha, J.P. and W. Sturges, 1978. Evidence for wind forced circulation in the Gulf of Mexico. Tech. rept., Dept. of Ocn., Fla. State Univ., pp. 134.

Bright, T.J. and R. Rezek, 1978. South Texas topographic features study. Final report to the U.S. Dept. of Int., Bur. of Land Management, OCS Office, N.O., La., p. 161.

Csanady, G.G., 1977. The coastal jet conceptual model in the dynamics of shallow seas. from "The Sea," Vol. 6, Marine Modeling. John Wiley and Sons, New York.

Franceschini, G.A., 1953. The distribution of mean monthly wind stress over the Gulf of Mexico. Sci. Report No. 1, Dept. of Ocn., Texas A&M Research Foundation, Texas A&M University, pp. 18.

Groves, G.W., 1955. Numerical filters for discrimination against tidal periodicities. Transactions, American Geophysical Union, Vol. 36, No. 6, 1073-1084.

Hann, R.W., et al., 1979. Evaluation of brine disposal from the Bryan mound site of the strategic petroleum reserve program, Texas A&M University, February 14, 1979.

Huyer, A. and J.G. Pattullo, 1972. A comparison between wind and current observations over the continental shelf off Oregon, summer 1969. JGR, 77(18), 3215-3220.

LaFond, E.C., 1951. Processing oceanographic data. U.S. Navy Hydrographic Office, H.O. Pub. No. 614, Washington, D.C.

Mayer, D.A., D.V. Hansen, and D.A. Ortman, 1979. Long term current and temperature observations on the middle Atlantic shelf, JGR, 84 (C4), 1776-1792.

Nowlin, W.D., Jr. and C.A. Parker, 1974. Effects of a cold-air outbreak on shelf waters of the Gulf of Mexico. J. of Phys. Ocn., 4(3), 467-486.

Officer, C.B. Physical Oceanography of Estuaries, John Wiley & Sons: New York, 1976.

Reid, J.L., I. Roden and J.G. Wyllie, 1958. Studies of the California current system. Calif. Coop. Ocn. Fish. Investigations, prog. rpt., July 1, 1966 to January 1, 1958. Contrib. from the Scripps Inst. of Ocn., New Series No. 998.

Reid, R.O. and B. Bodine, 1968. Numerical model for storm surges in Galveston Bay. J. of the Waters and Harbors Division, Proc. of the Am. Soc. of Civil Eng.

Zetler, B.D. and D.V. Hansen, 1972. Tides in the Gulf of Mexico. Texas A&M University Oceanographic Studies, Vol. 2 (Capurro and Reid, eds.), 265-275.

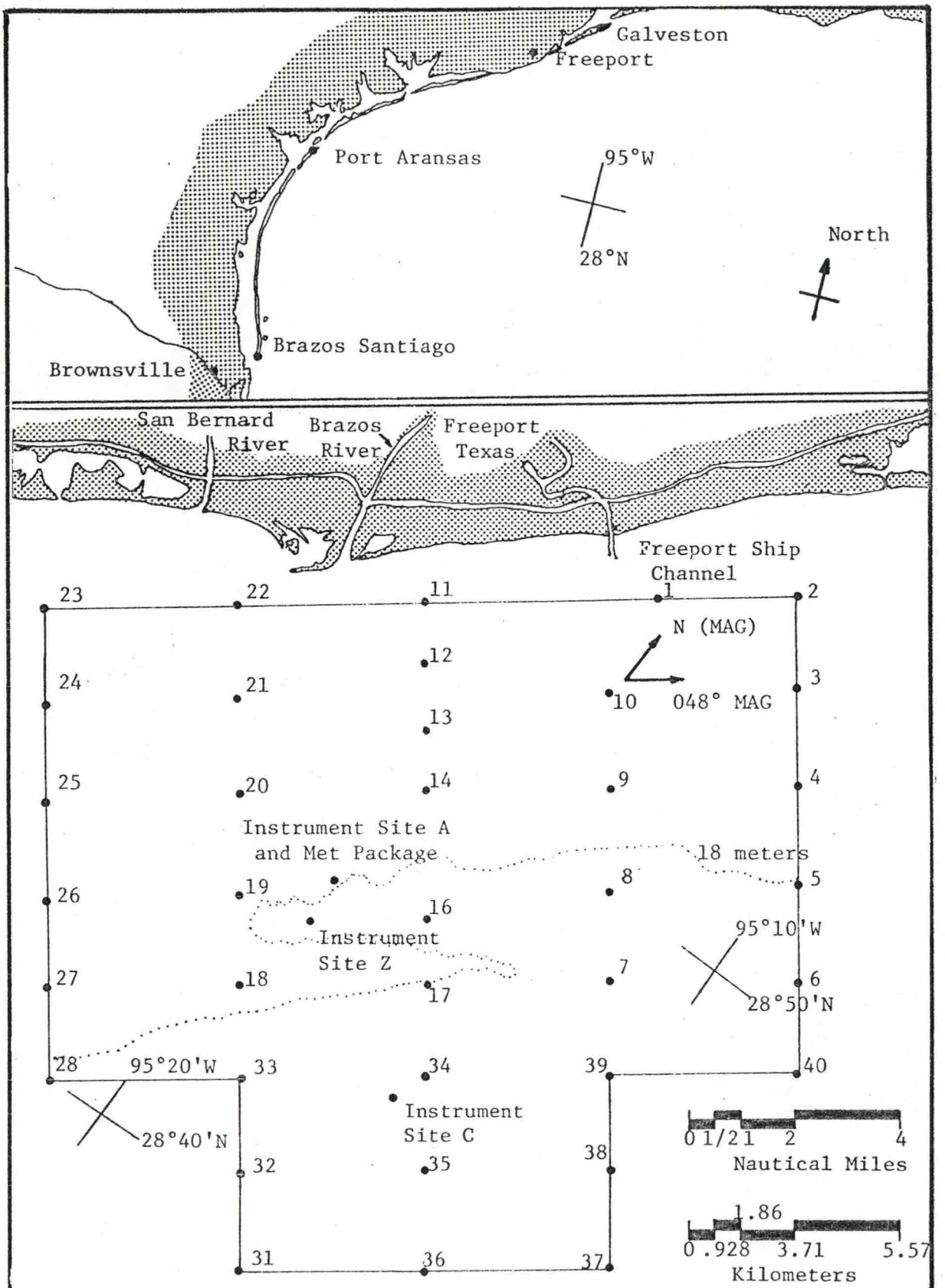

Fig. I-1. Location of study area and sites of data collection.

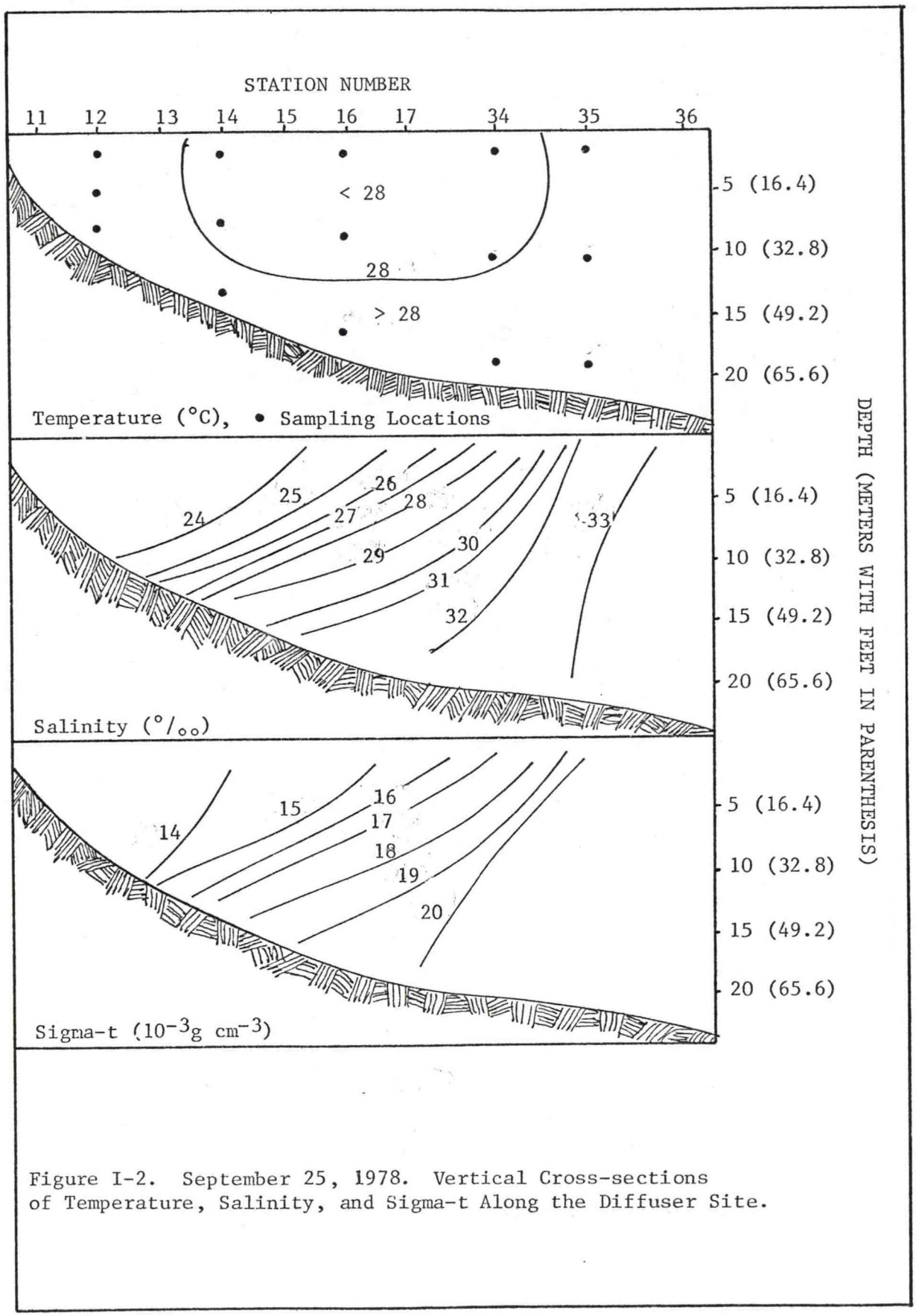

Figure I-2. September 25, 1978. Vertical Cross-sections of Temperature, Salinity, and Sigma-t Along the Diffuser Site.

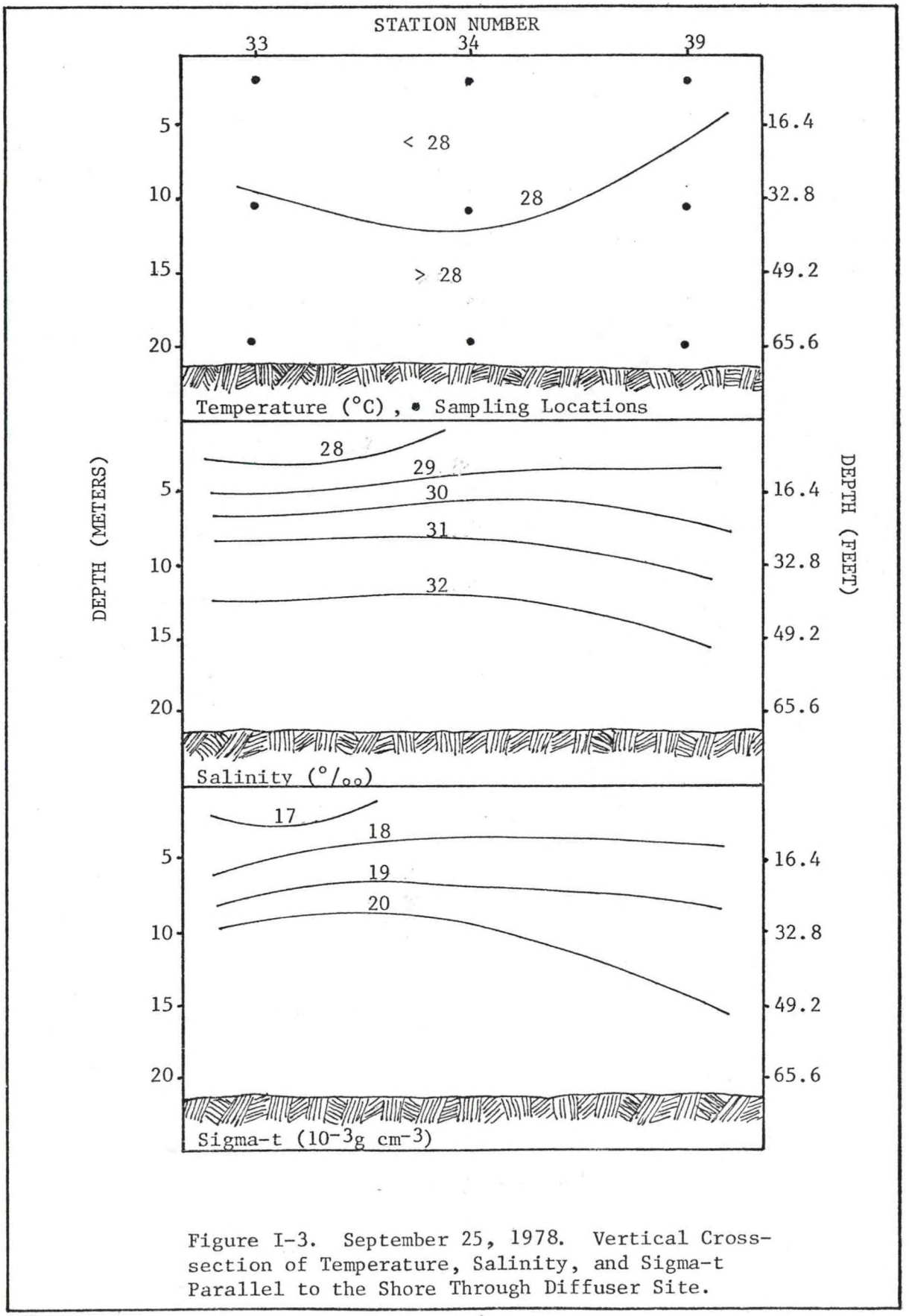

Figure I-3. September 25, 1978. Vertical Cross-section of Temperature, Salinity, and Sigma-t Parallel to the Shore Through Diffuser Site.

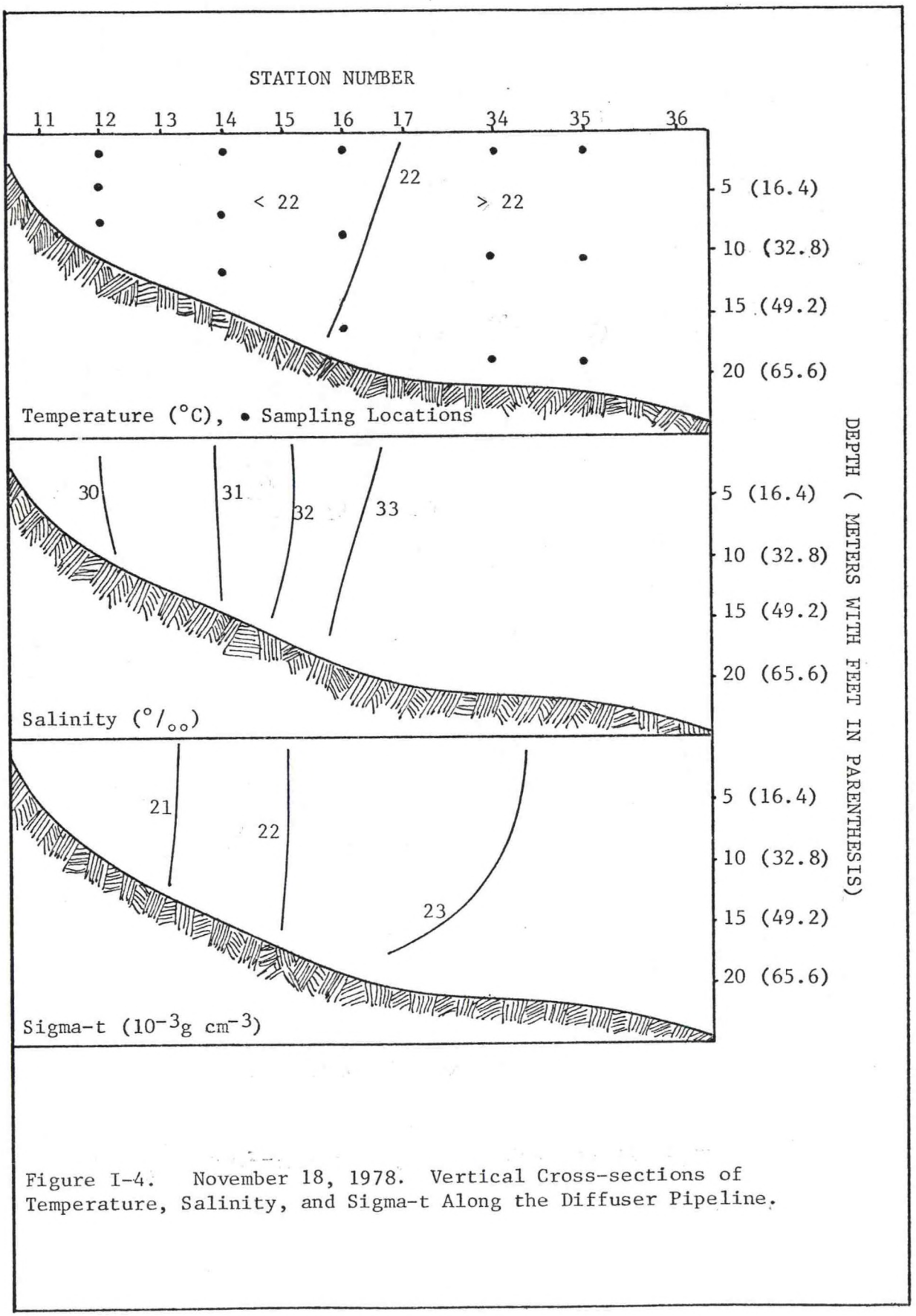

Figure I-4. November 18, 1978. Vertical Cross-sections of Temperature, Salinity, and Sigma-t Along the Diffuser Pipeline.

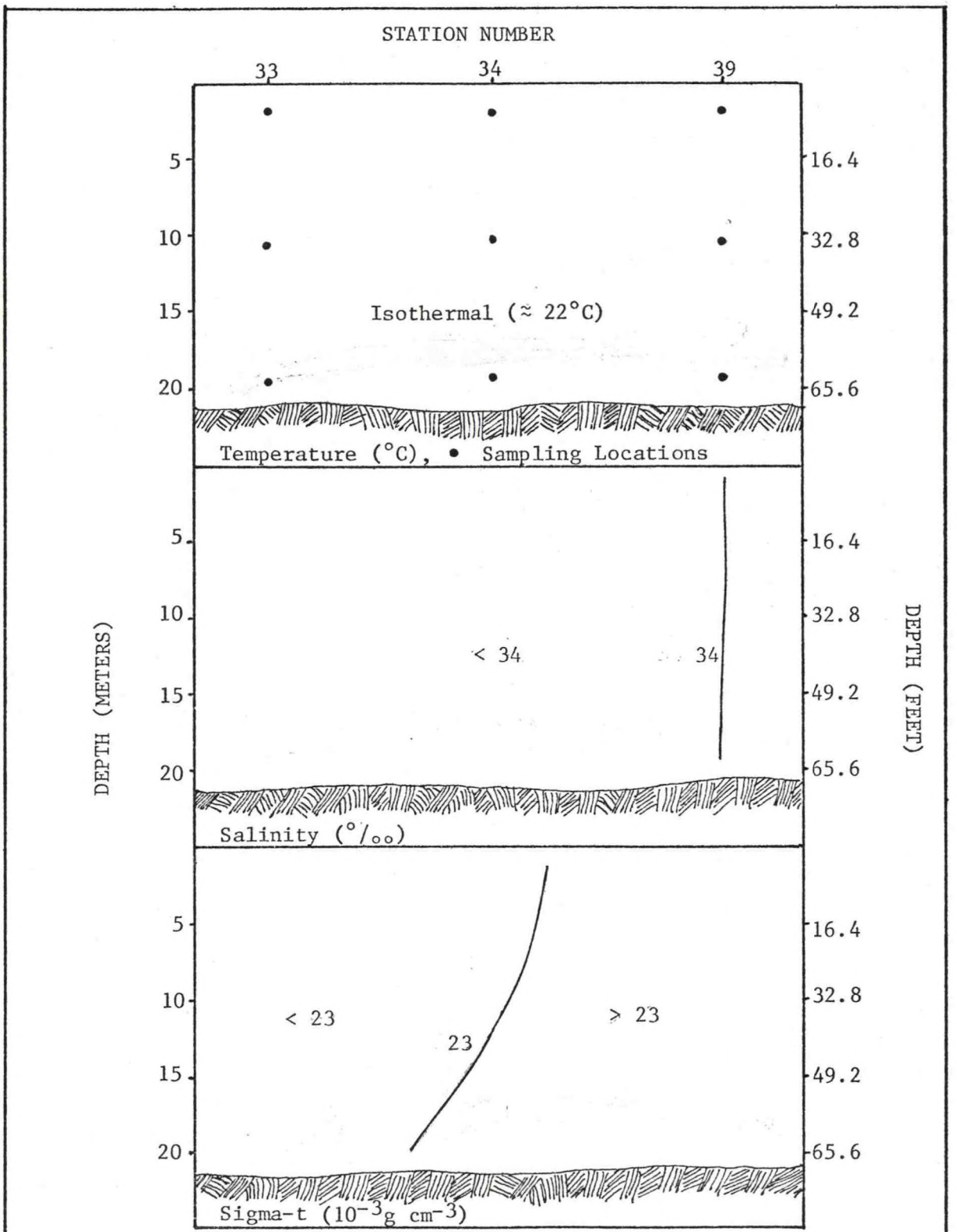

Figure I-5. November 18, 1978. Vertical Cross-sections of Temperature, Salinity, and Sigma-t Parallel to Shore Through the Diffuser Site.

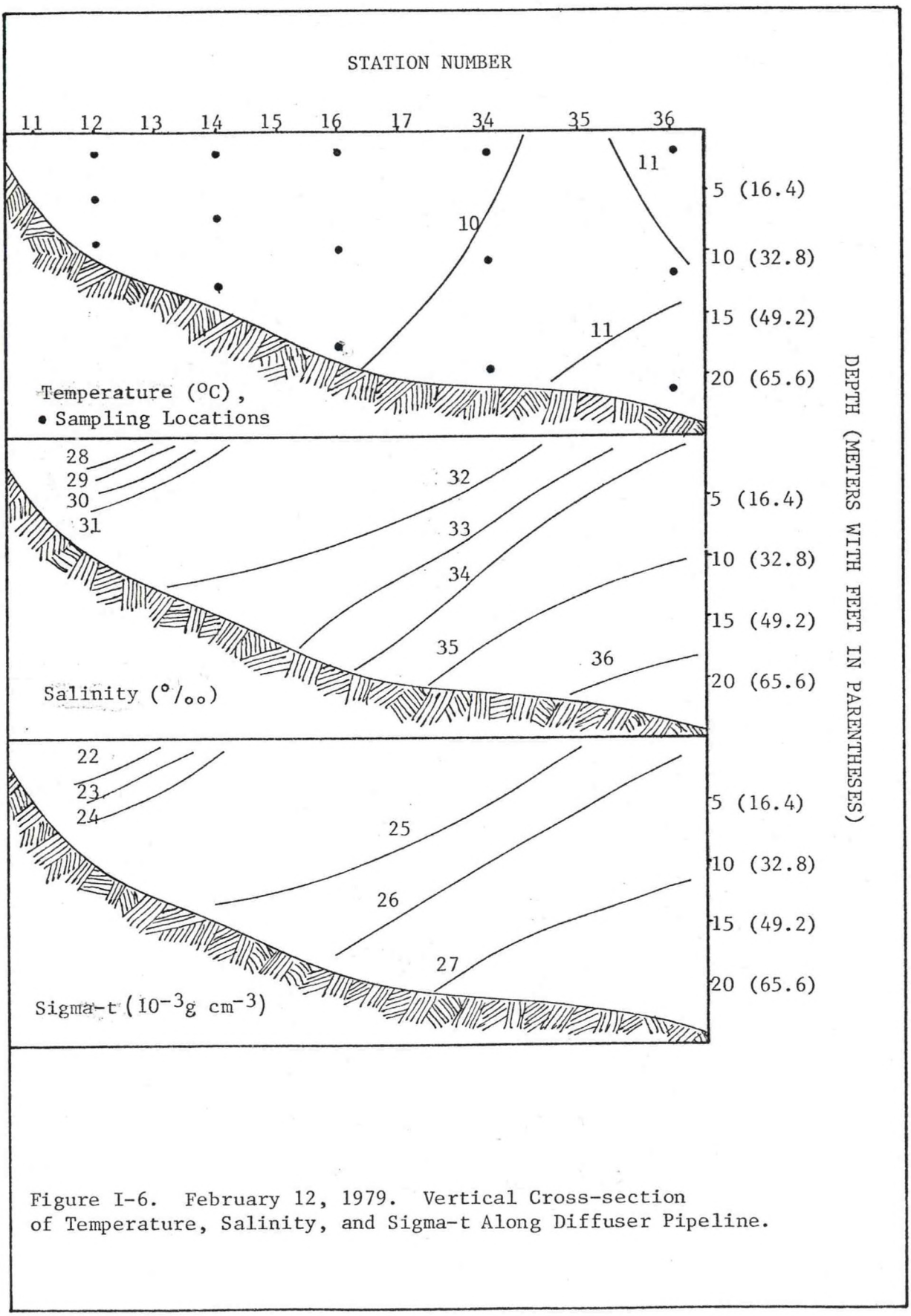

Figure I-6. February 12, 1979. Vertical Cross-section of Temperature, Salinity, and Sigma-t Along Diffuser Pipeline.

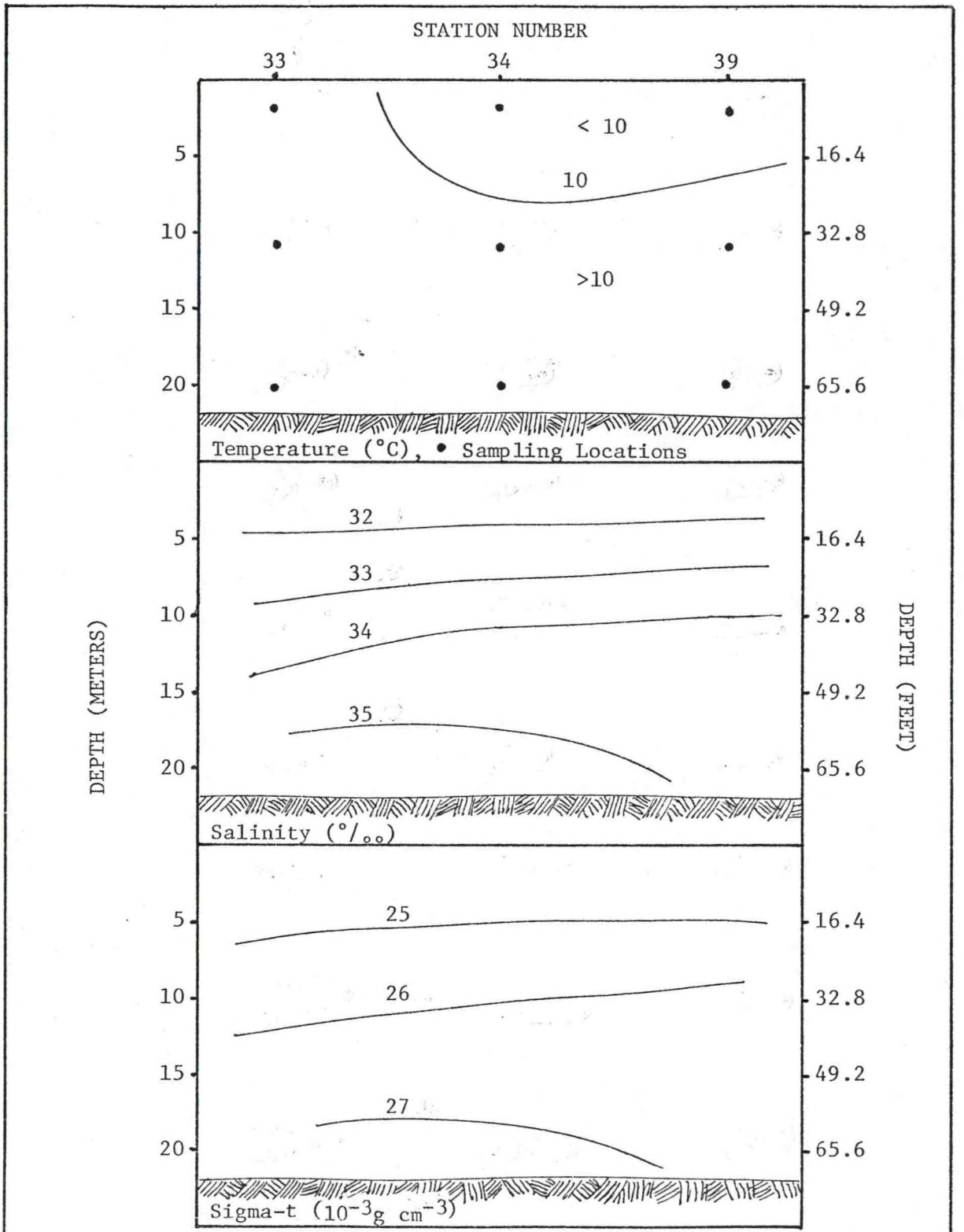

Figure I-7. February 12, 1979. Vertical Cross-section of Temperature, Salinity, and Sigma-t Parallel to Shore Through Diffuser Site.

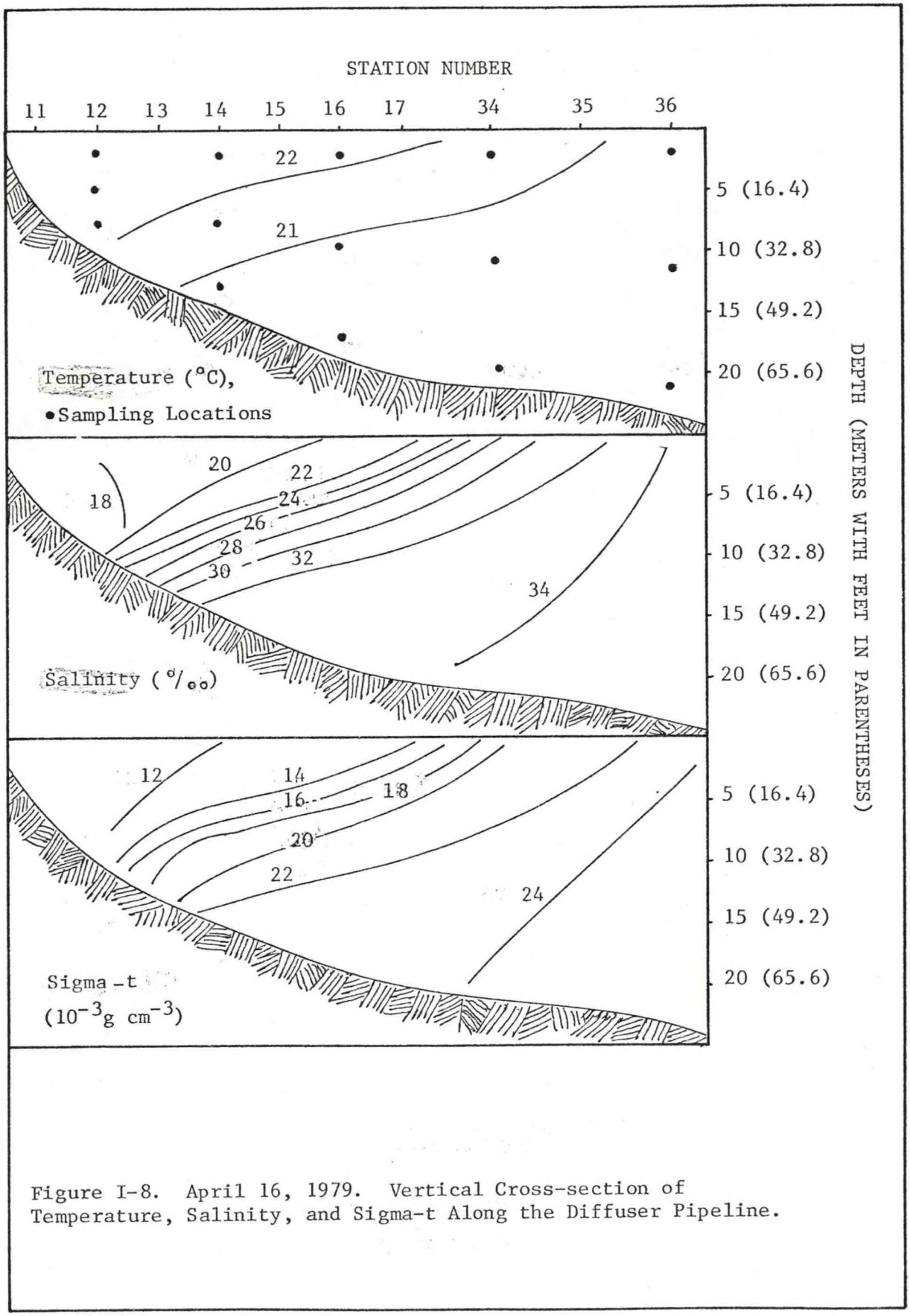

Figure I-8. April 16, 1979. Vertical Cross-section of Temperature, Salinity, and Sigma-t Along the Diffuser Pipeline.

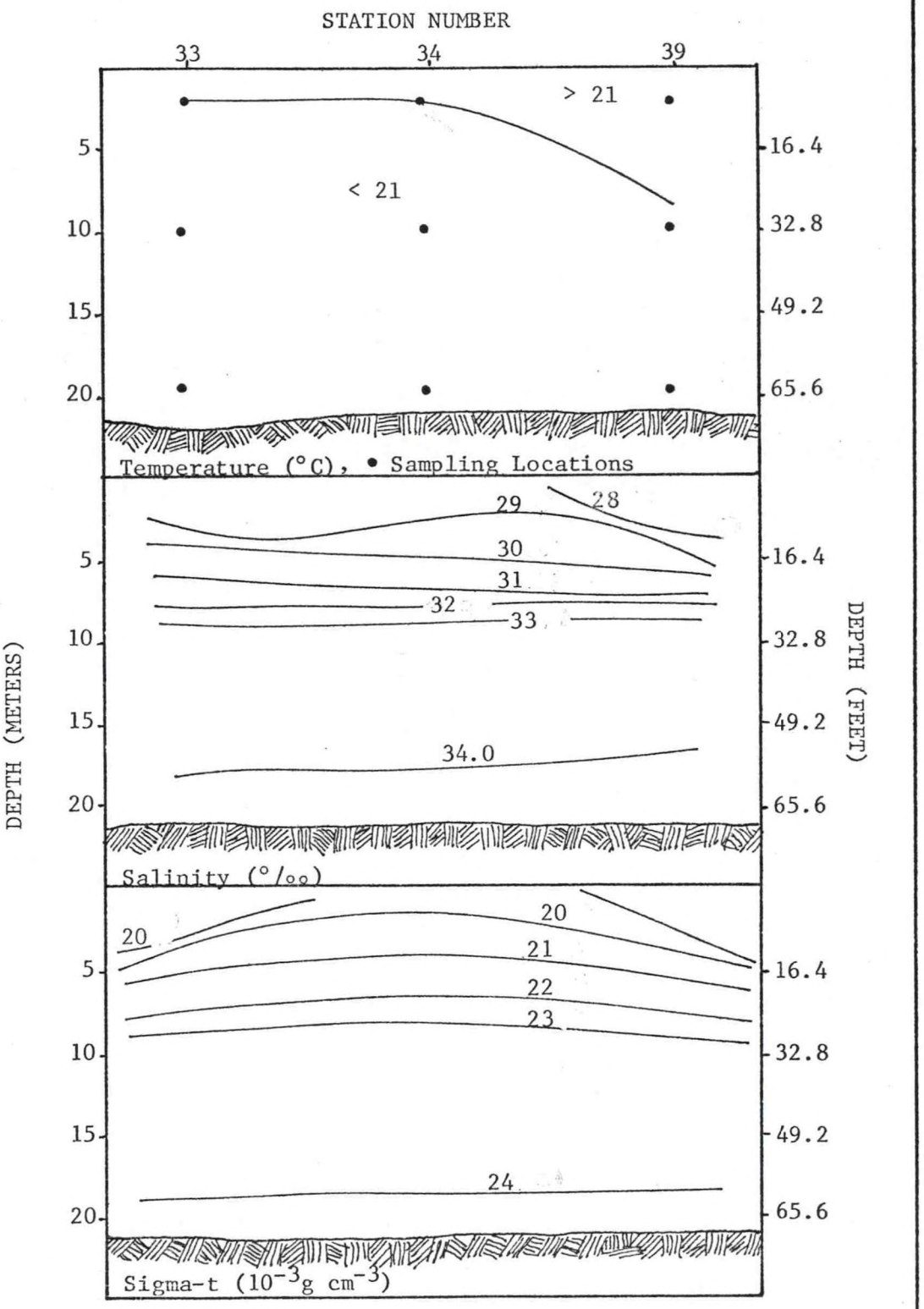

April 16, 1979

Figure I-9. April 16, 1979. Vertical Cross-section of Temperature, Salinity, and Sigma-t Parallel to Shore Through Diffuser Site.

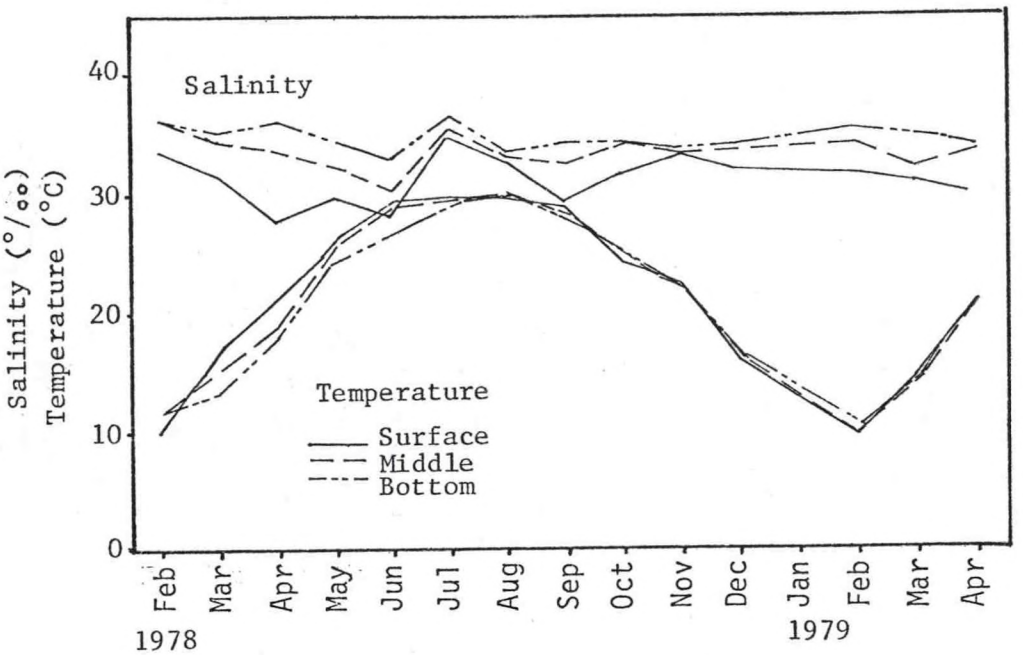

Figure I-10. Average Temperature and Salinity Versus Month of Year at Diffuser Site (Station MM).

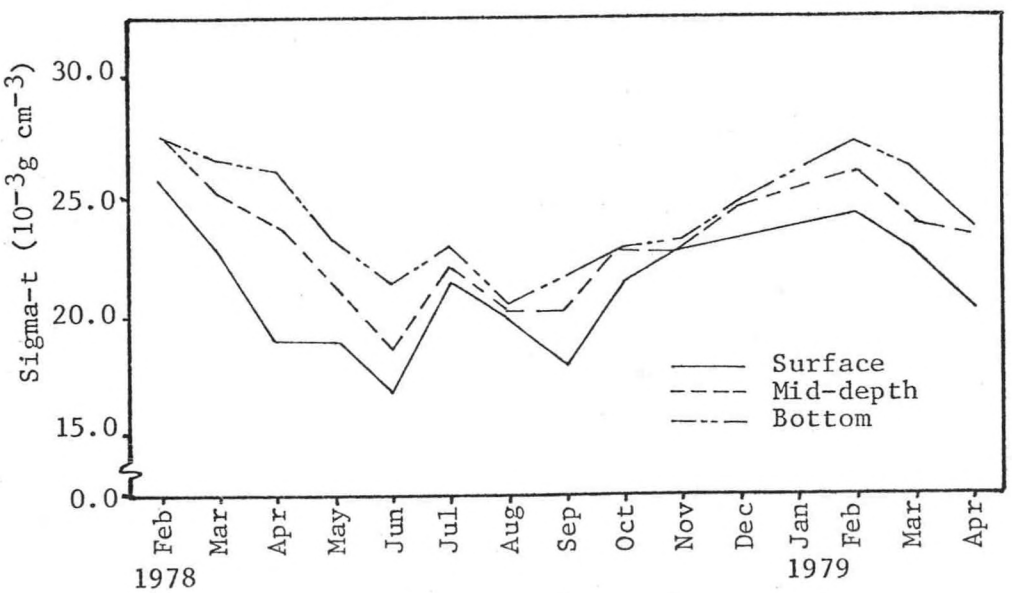

Figure I-11. Average Sigma-t Versus Month of Year at Diffuser Site (Station MM).

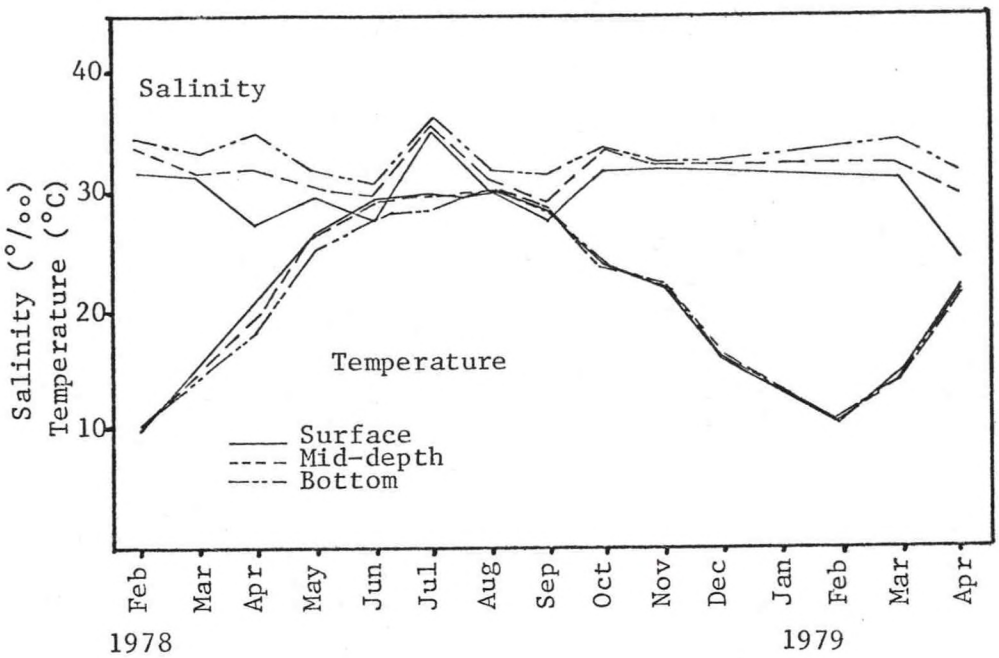

Figure I-12. Average Salinity and Temperature for Stations 9, 12, 14, 16, 20, 33, 34, 36, and 39 Versus Month of Year.

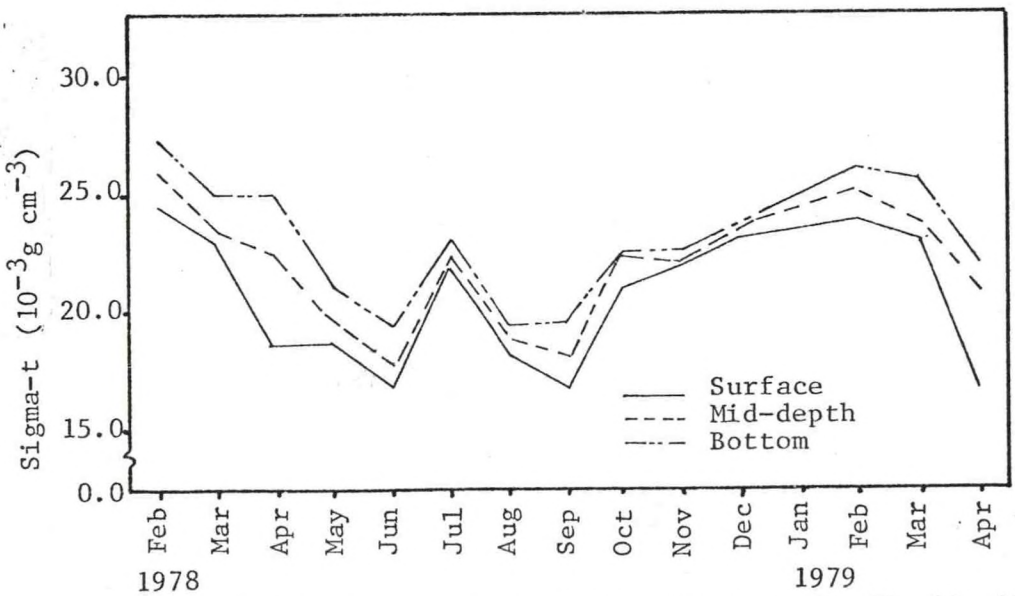

Figure I-13. Average Sigma-t for Stations 9, 12, 14, 16, 20, 33, 34, 36, and 39 Versus Month of Year.

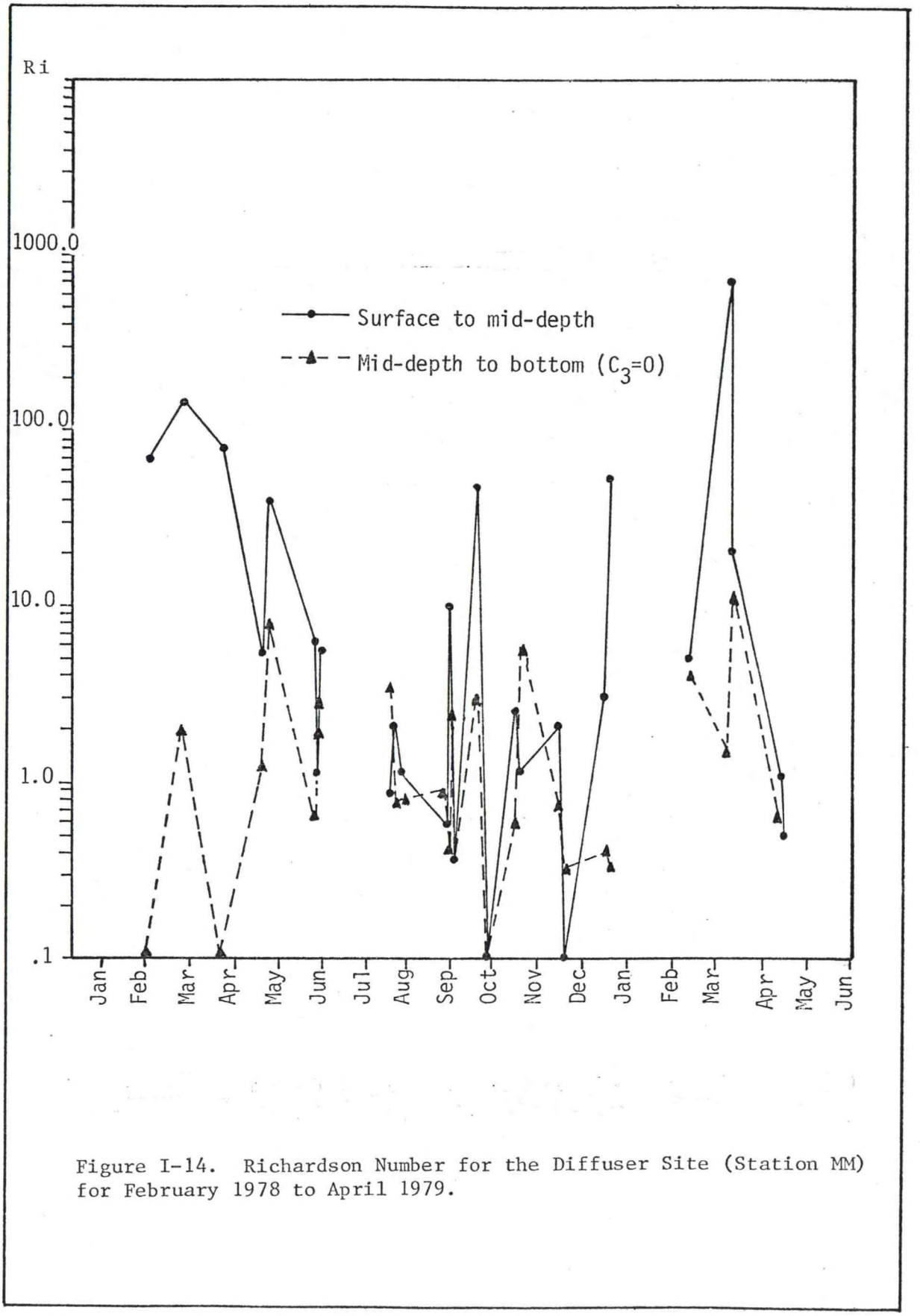

Figure I-14. Richardson Number for the Diffuser Site (Station MM) for February 1978 to April 1979.

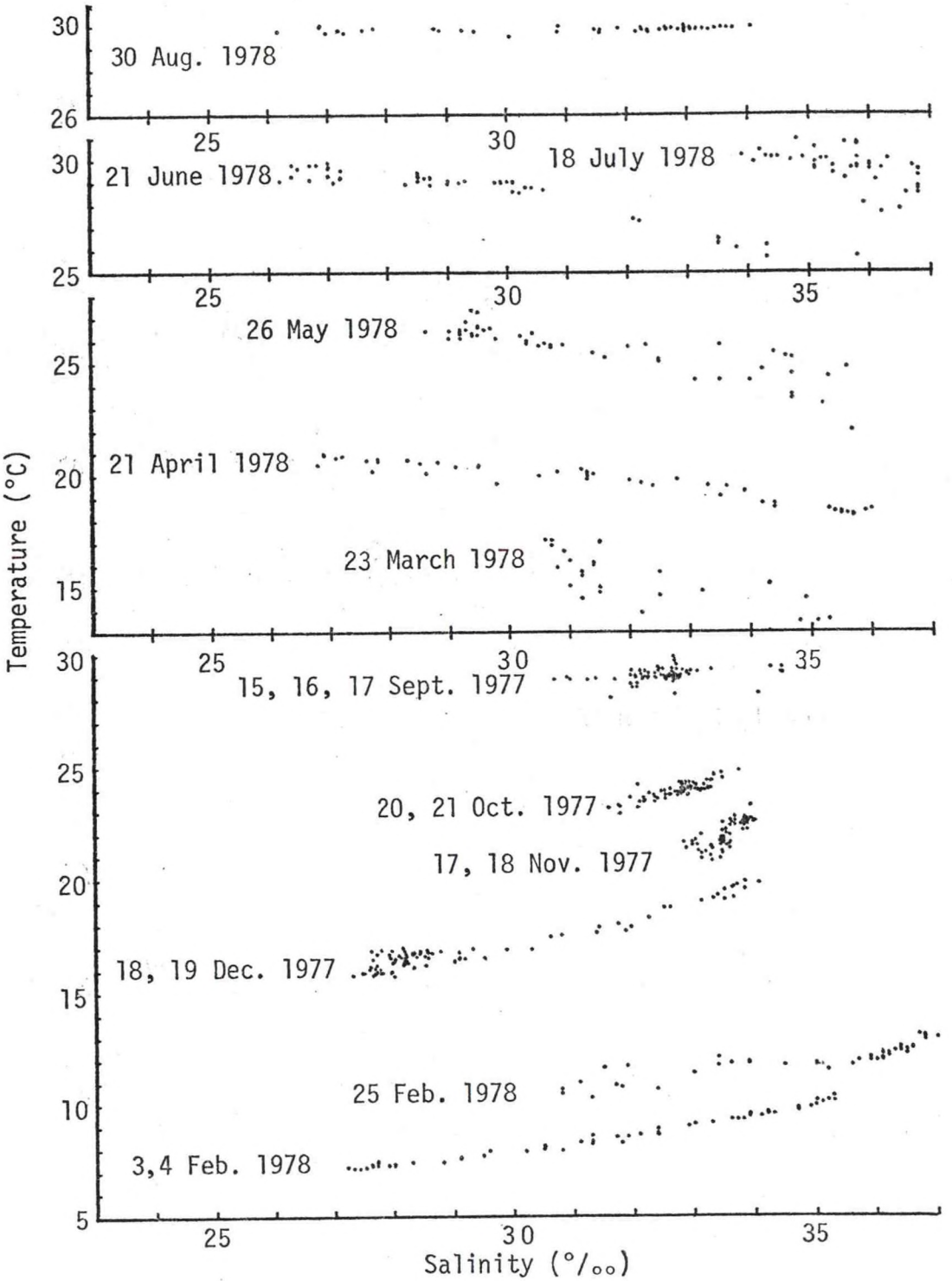

Figure I-15. Temperature-salinity relationships from September 1977 through August 1978.

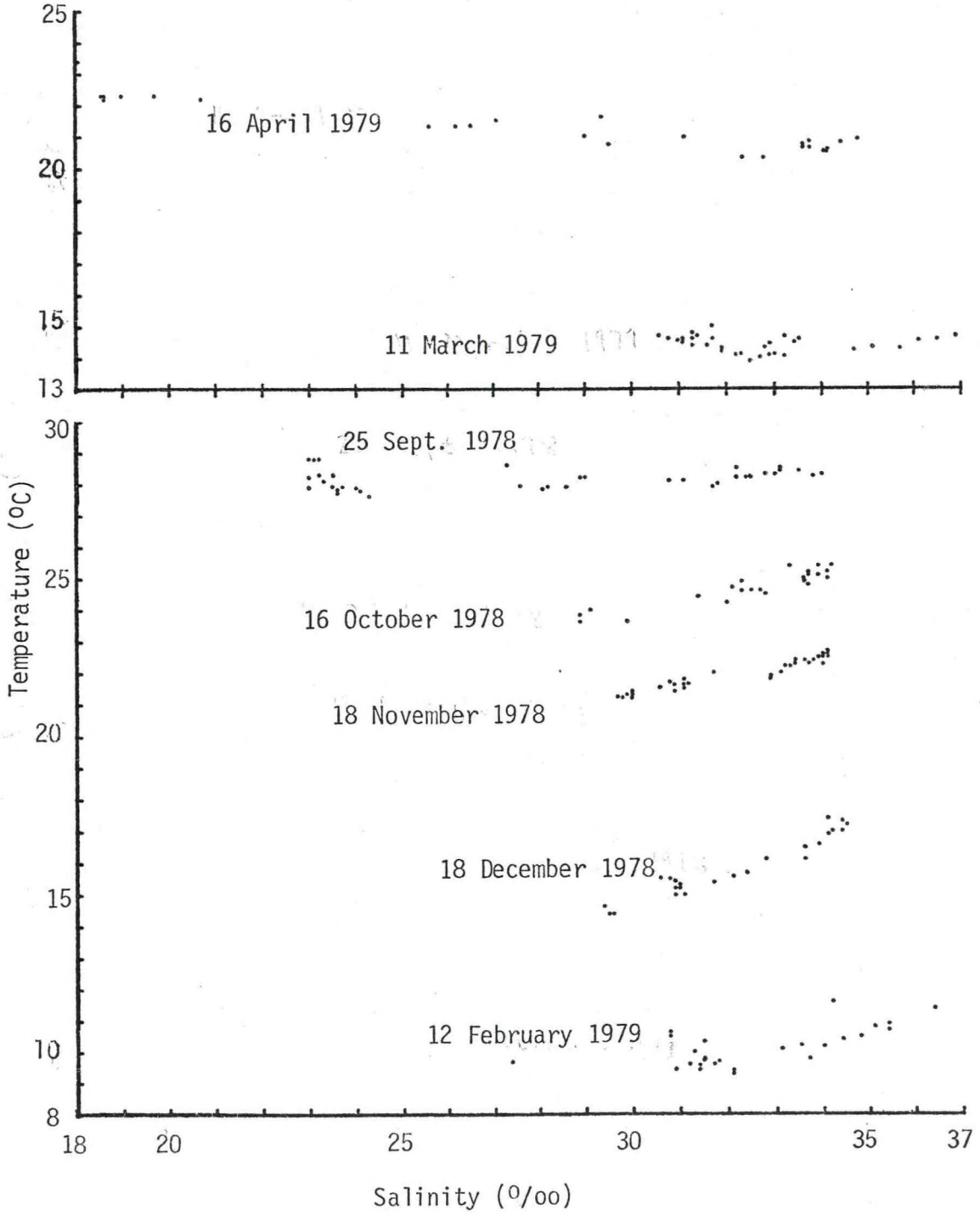

Figure I-16. Temperature-salinity relationships from September 1978 through April 1979.

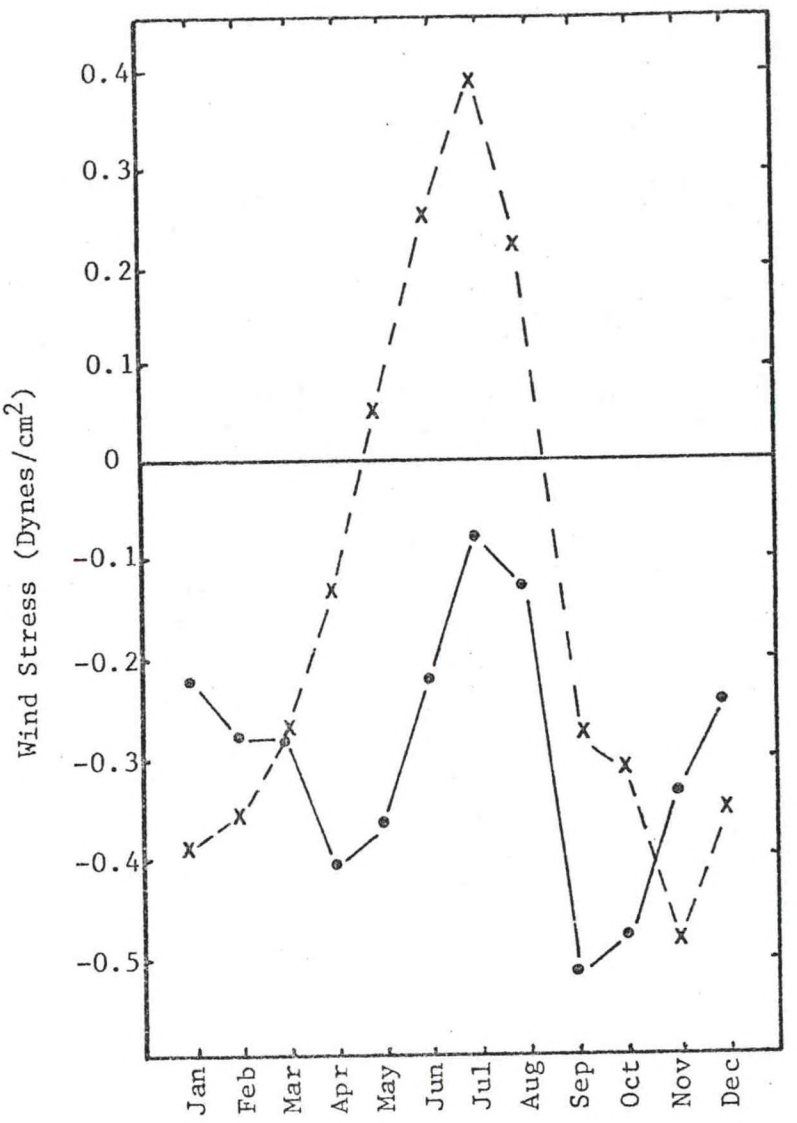

Fig. I-17. Mean monthly values of longshore wind stress at Galveston, Texas. The x's indicate 15 year means (July 1948-September 1963) for wind data collected at Schole's Field in Galveston. The ·'s indicate 20 year means for ship observed winds near Galveston (Blaha and Sturges, 1978).

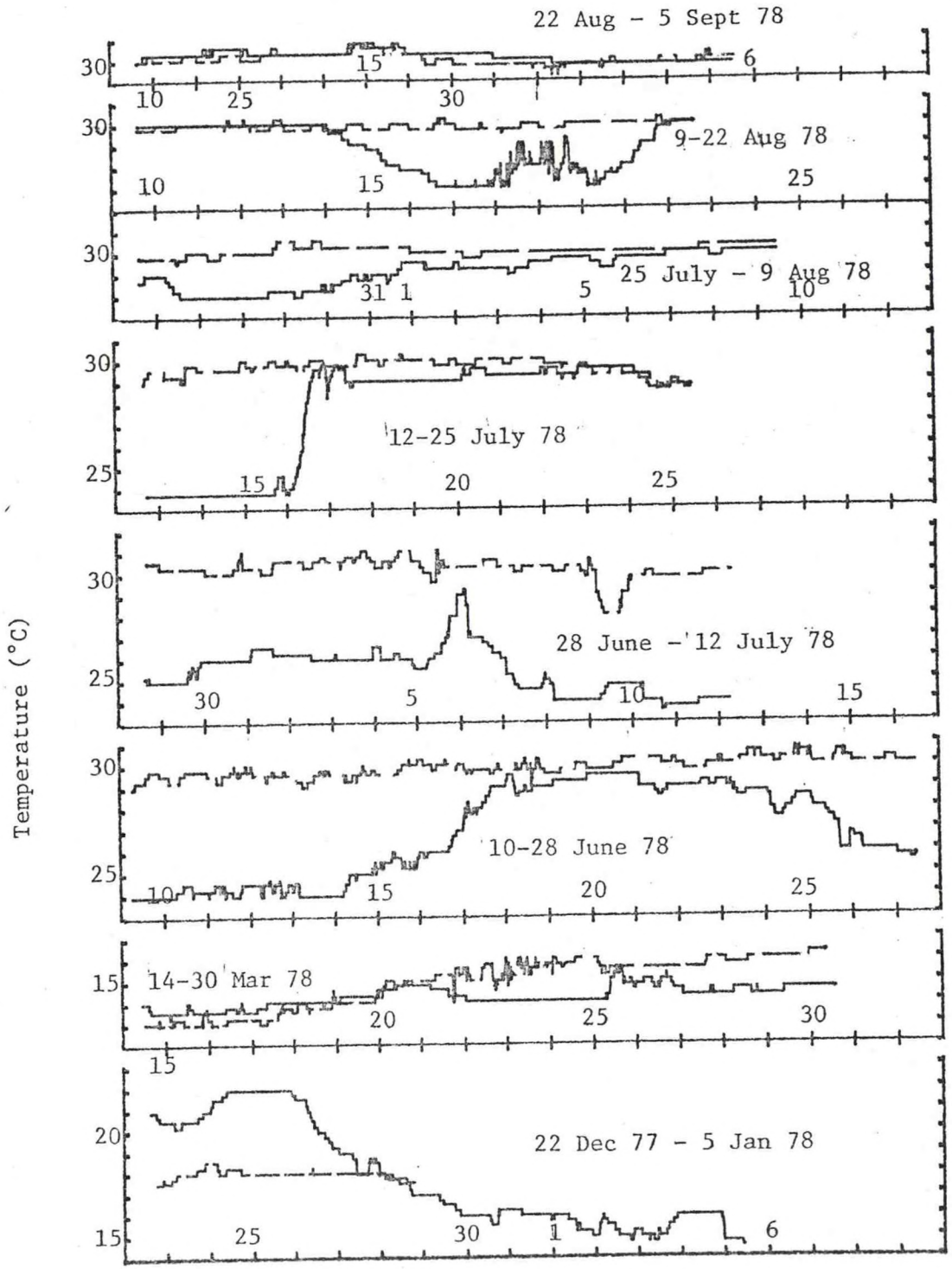

Figure I-18a. Surface (dashed lines) and bottom (solid lines) thermograph data from site A, for indicated periods between December 1977 and September 1978. Water depth is 17 m.

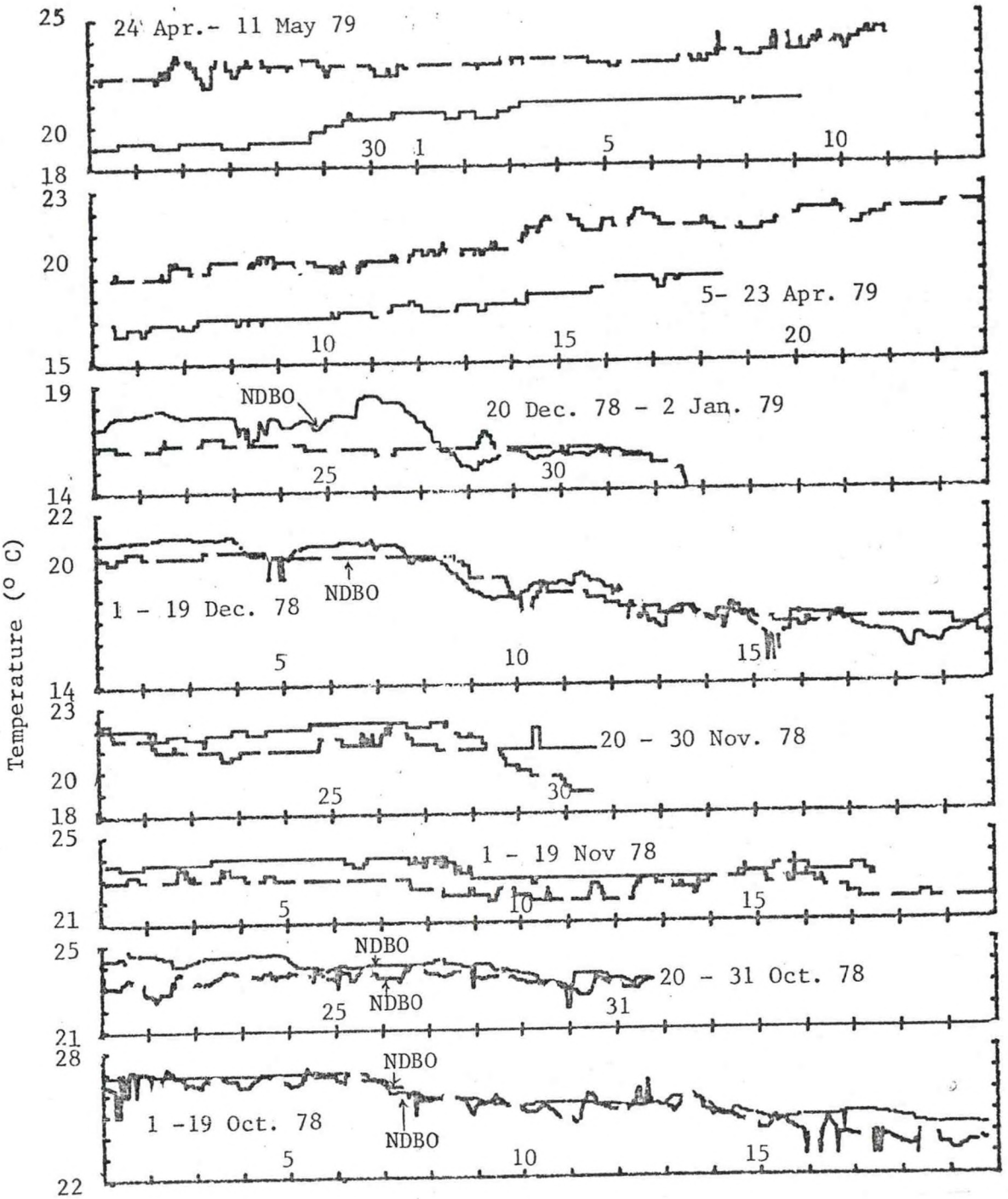

Figure I-18b. Surface (dashed lines) and bottom (solid lines) thermograph data from site A, for indicated periods between October 1978 and May 1979. Water depth is 17 m. NDBO data is used for the top or bottom data or both when the TAMU thermographs malfunctioned or were lost at sea.

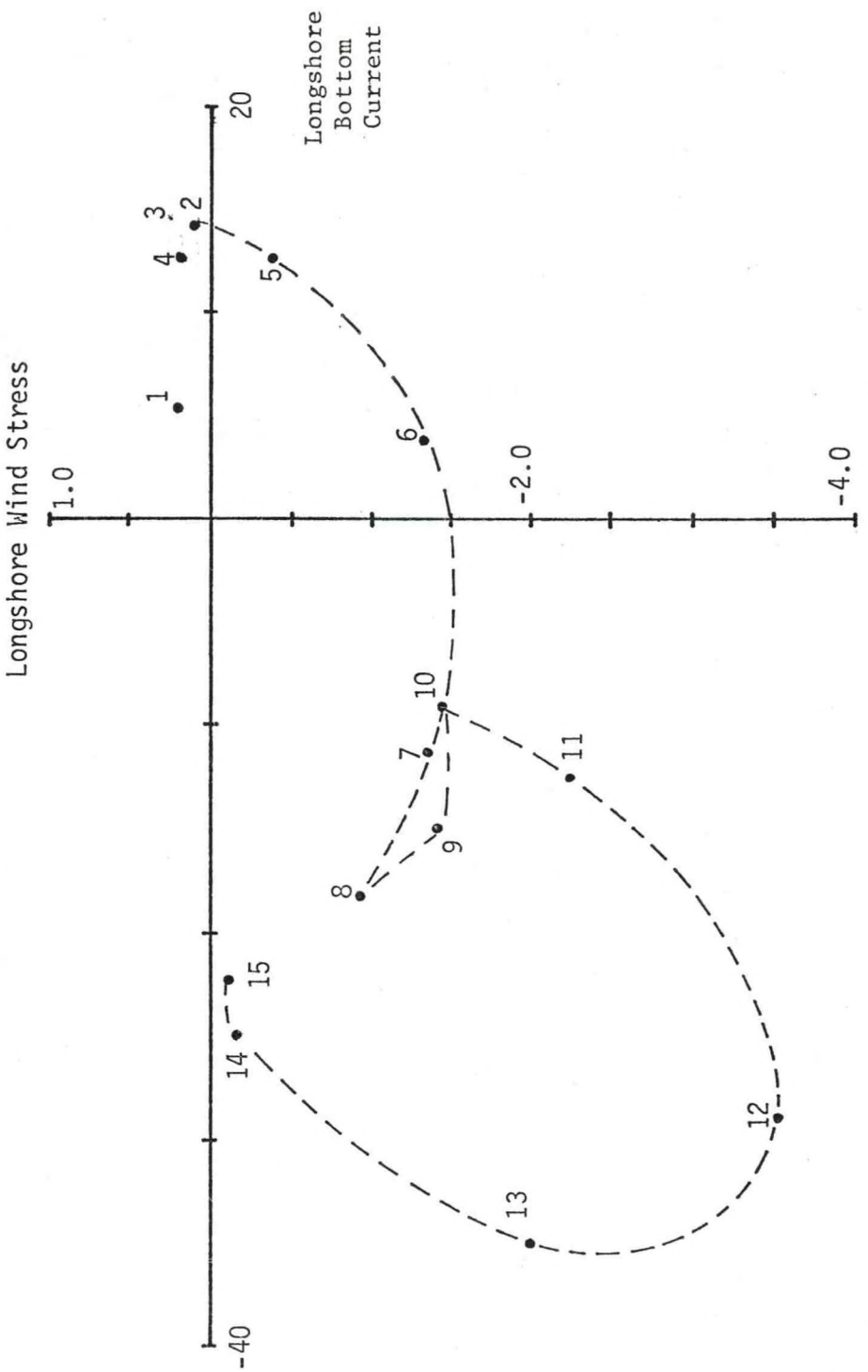

Figure I-19. A plot of 12 hour averages of filtered longshore wind stress (dynes/cm^2) and corresponding filtered longshore bottom current (cm/s) for 22-30 December 1977.

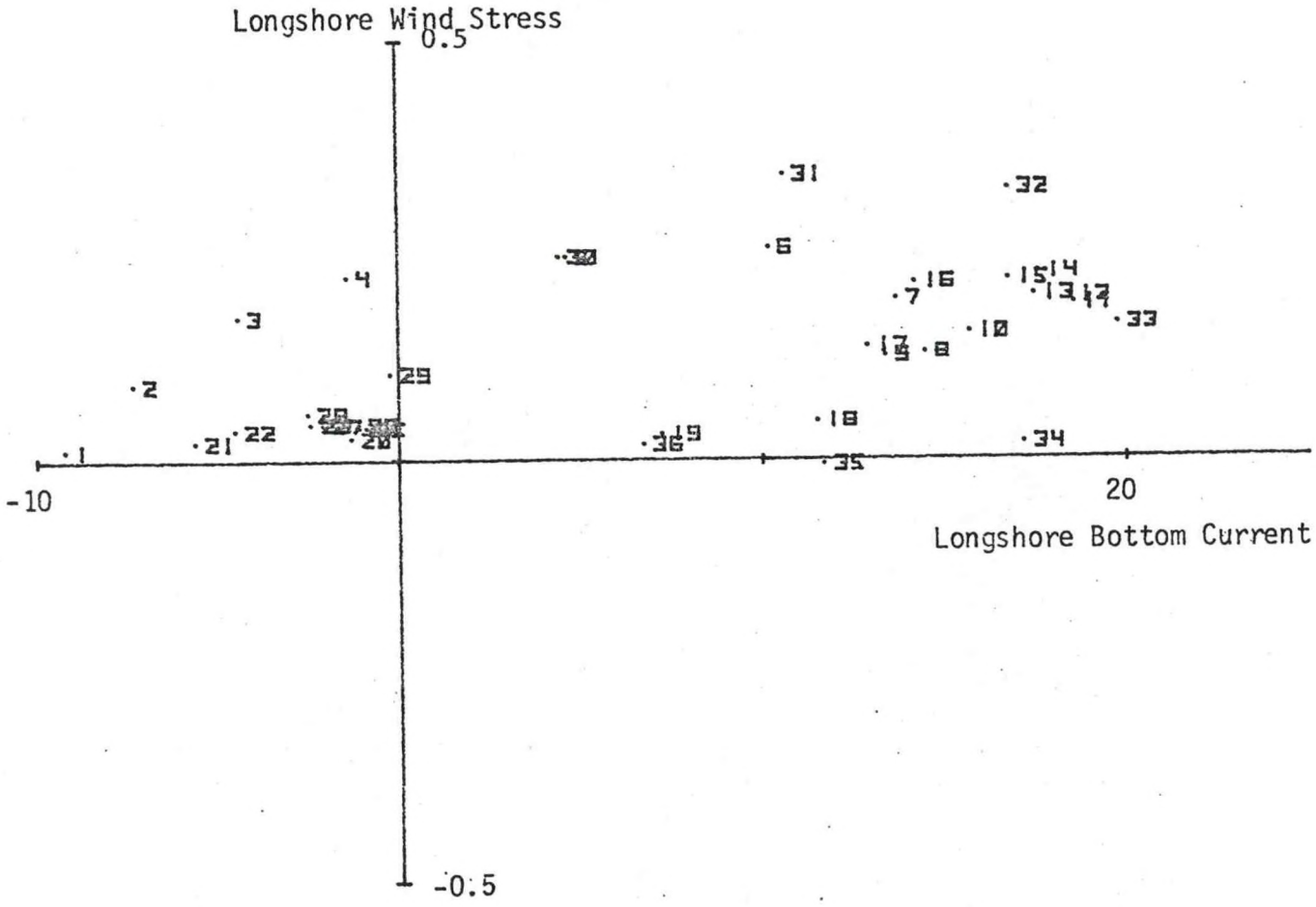

Figure I-20. A plot of 12 hour averages of filtered longshore wind stress (dynes/cm^2) and corresponding filtered longshore bottom current (cm/s) for 30 June-16 July 1978.

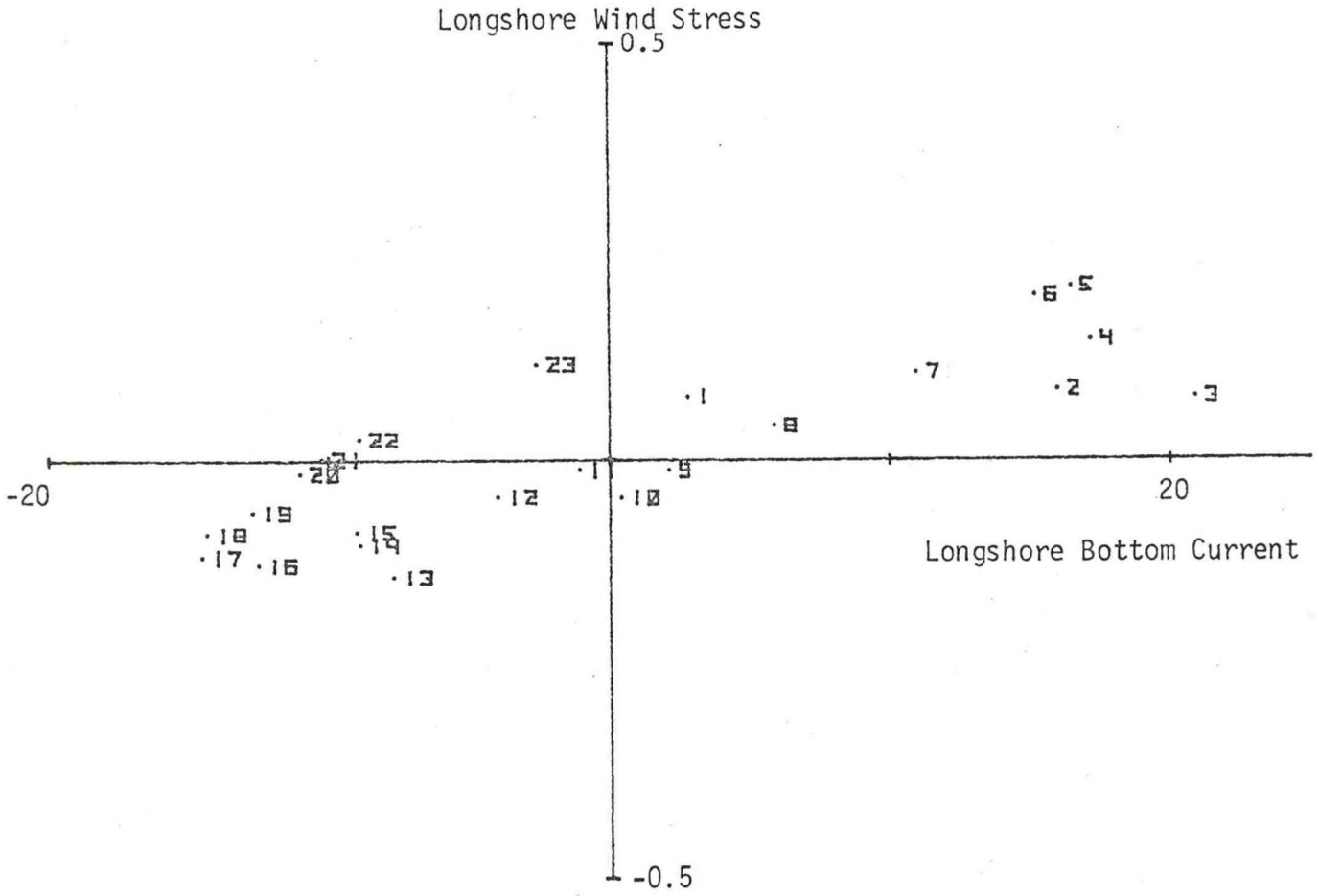

Figure I-21. A plot of 12 hour averages of filtered longshore wind stress (dynes/cm^2) and corresponding filtered longshore bottom current (cm/s) for 29 July-9 August 1978.

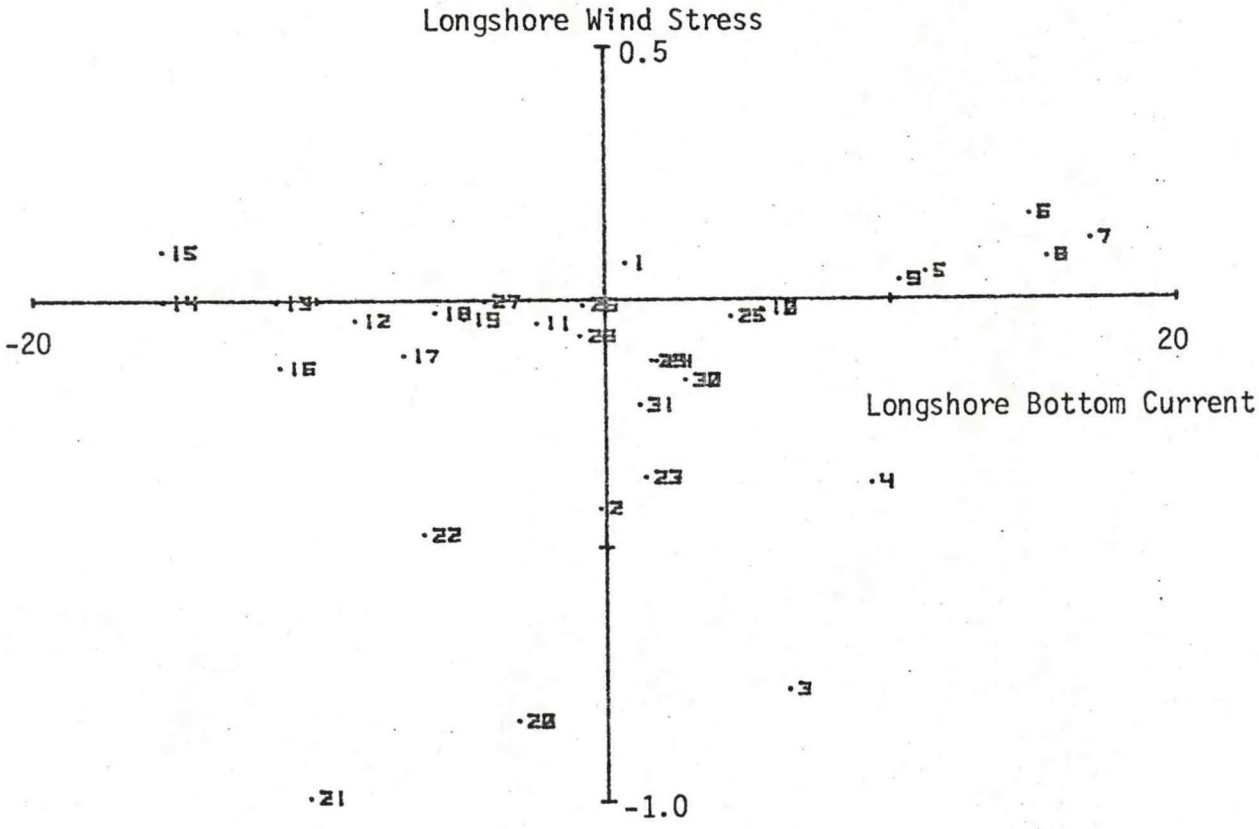

Figure I-22. A plot of 12 hour averages of filtered longshore wind stress (dynes/cm^2) and corresponding filtered longshore bottom current (cm/s) for 14-30 March 1978.

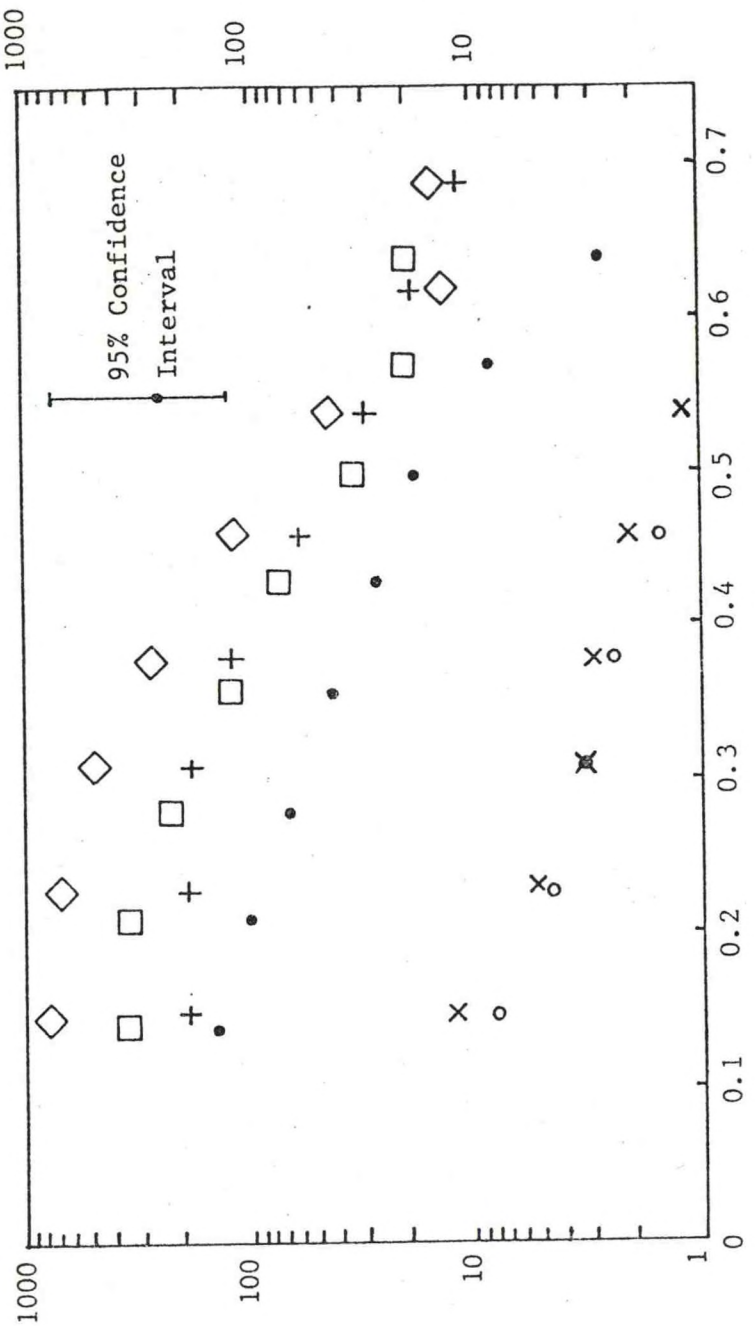

Figure I-23. Power spectra for filtered wind stress data for 30 June-5 September 1978 (X, ○), 18 October-31 December 1978 (●, □), and 30 November 1978-5 February 1979 (+ , ◇). Longshore components are represented by X , ● , and + , and cross-shelf by ○ , □ , and ◇ .

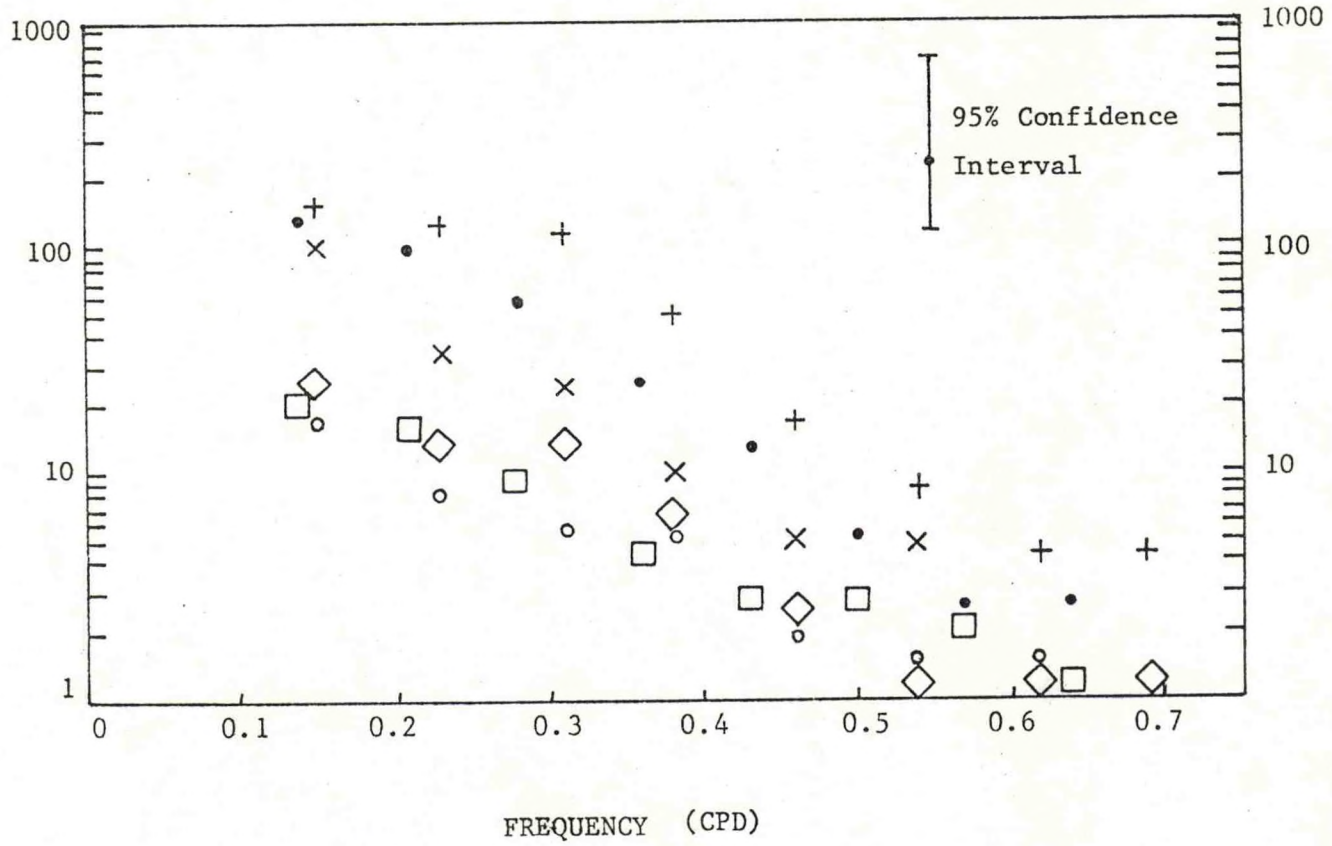

Figure I-24. Power spectra for filtered surface current data for 30 June-5 September 1978 (X , o), 18 October-31 December 1978 (• , □), and 30 November 1978-5 February 1979 (+ , ◇). Longshore components are represented by x , • , and + , and cross-shelf by o , □ , ◇ .

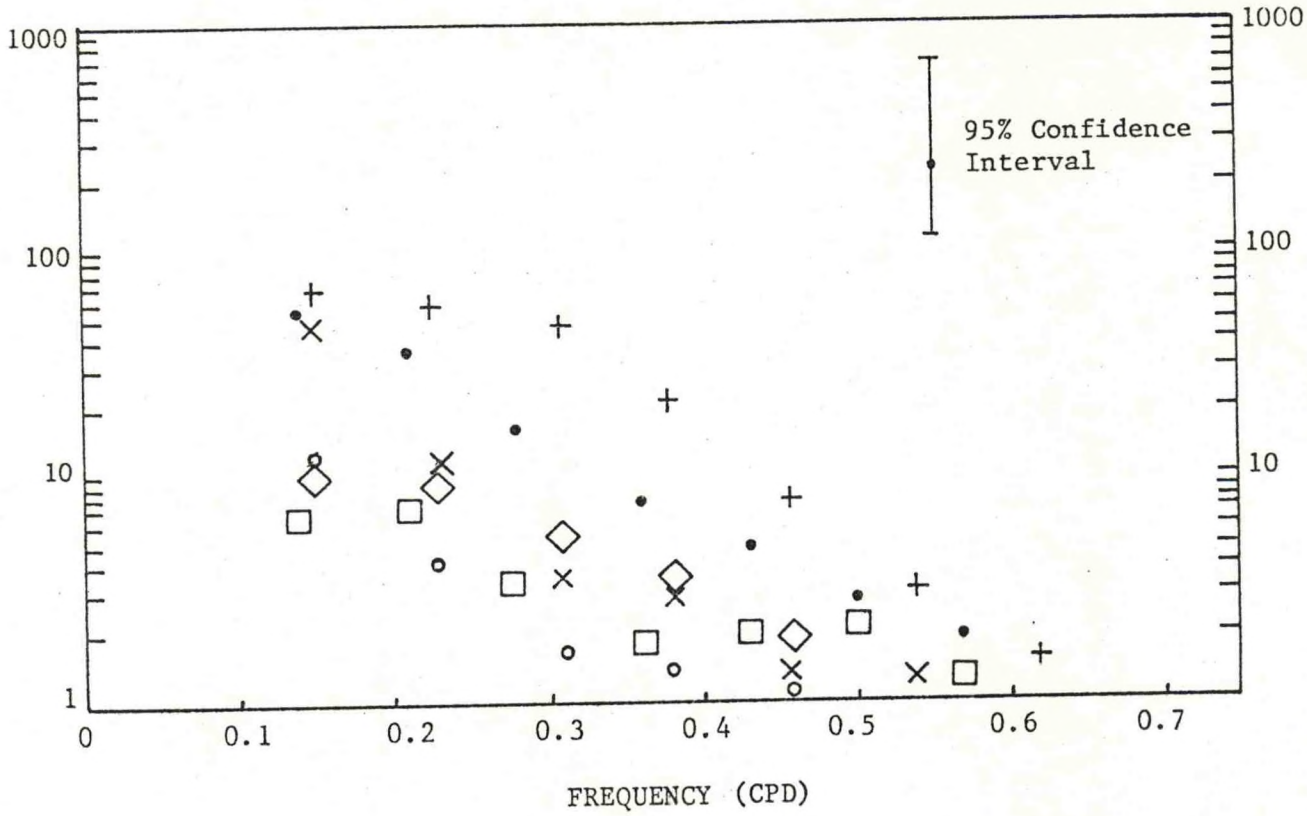

Figure I-25. Power spectra for filtered bottom current data for 30 June-5 September 1978 (X , ○), 18 October-31 December 1978 (● , □), and 30 November 1978-5 February 1979 (+ , ◇). Longshore components are represented by X , ● , and + , and cross-shelf by ○ , □ , ◇ .

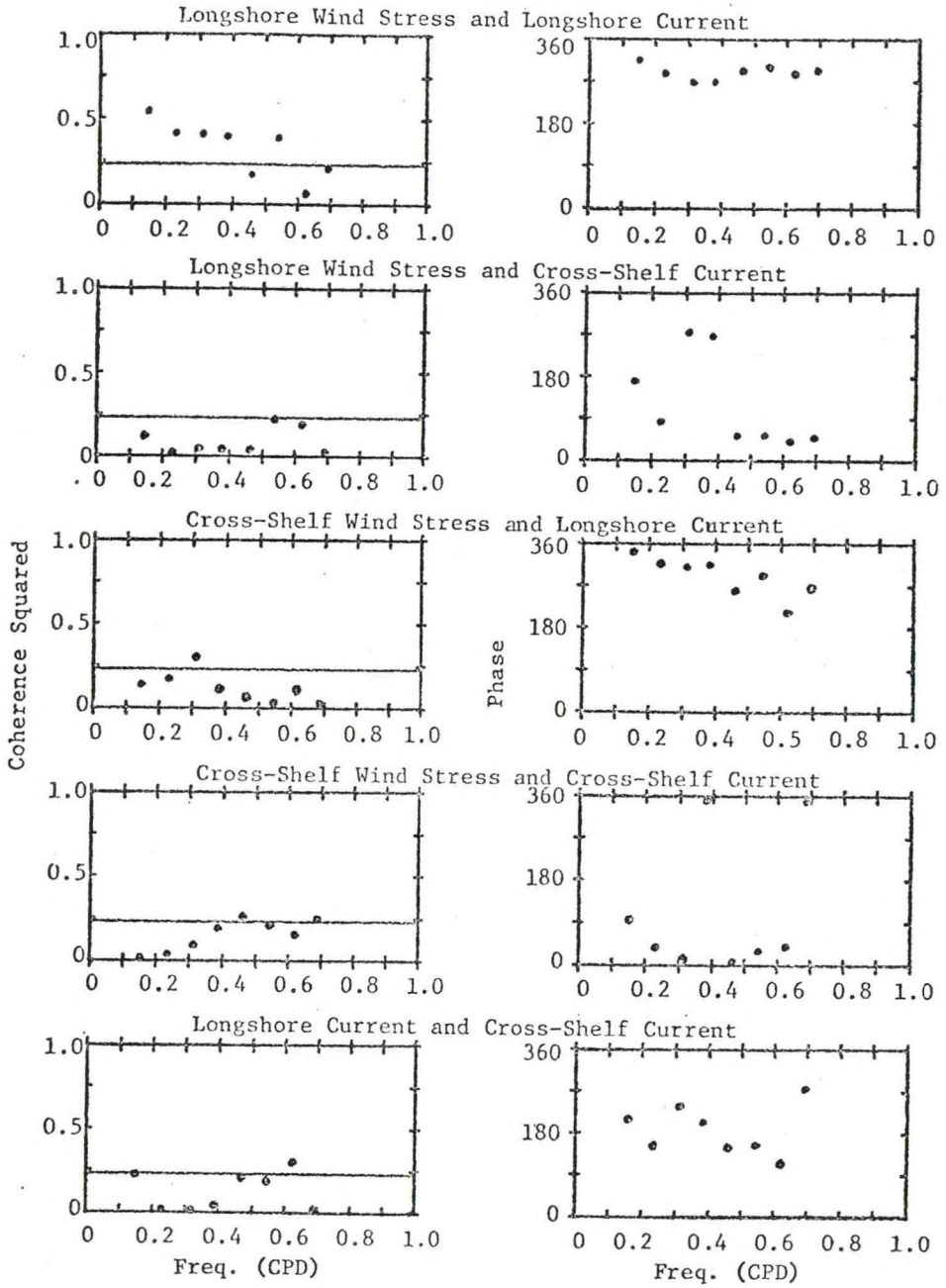

Figure I-26. Coherence squared and phase (in degrees) spectra between wind stress and surface current components for 30 June-5 September 1978. The line across the coherence squared is the 90% confidence limit. The 95% confidence interval for the phases is a maximum of ±46°. Larger coherence squared values will have smaller confidence intervals for the corresponding phase.

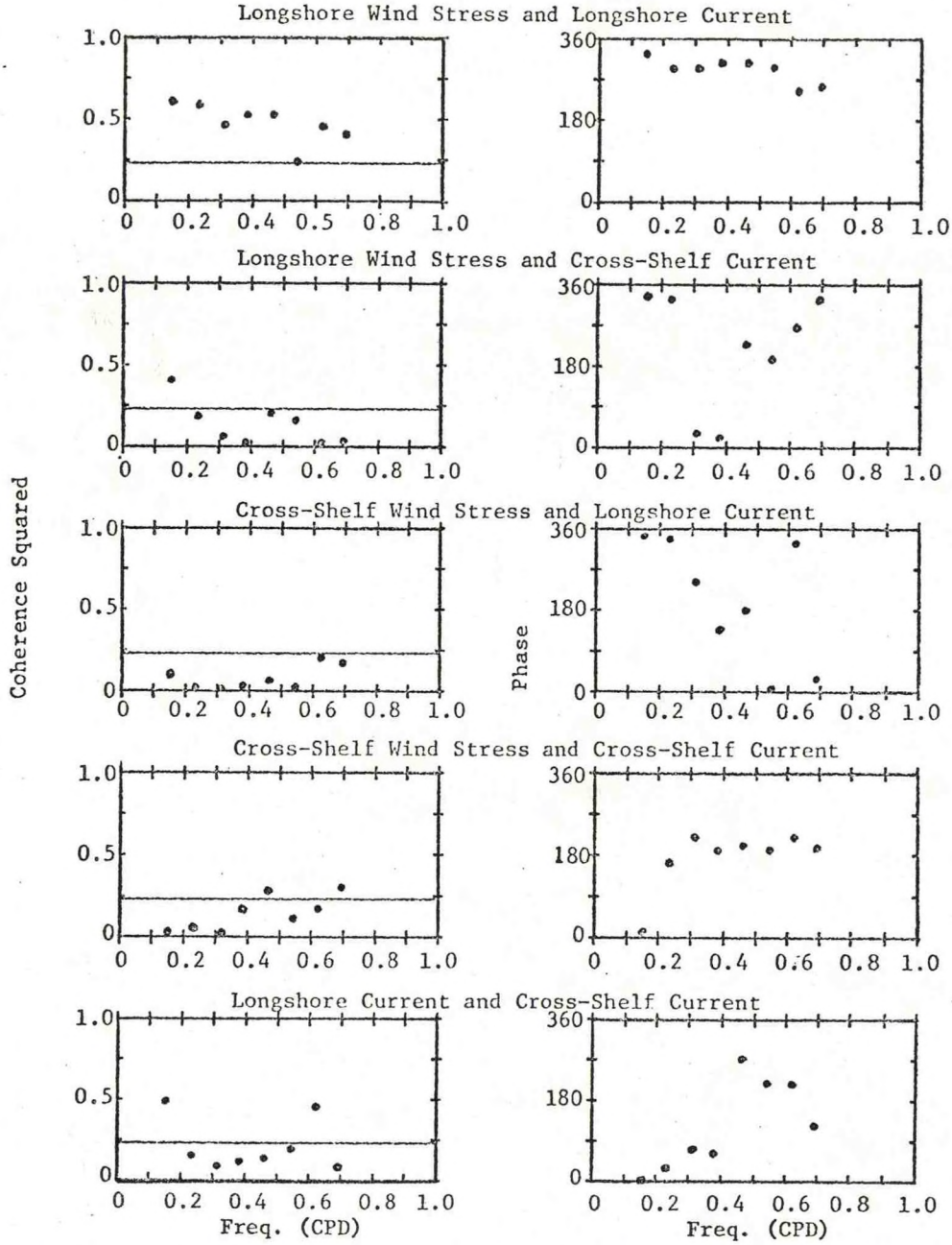

Figure I-27. Coherence squared and phase (in degrees) spectra between wind stress and bottom current components for 30 June-5 September 1978. The line across the coherence squared is the 90% confidence limit, and the 90% confidence interval for the phases is ±46°. Larger coherence squared values will have smaller confidence intervals for the corresponding phase.

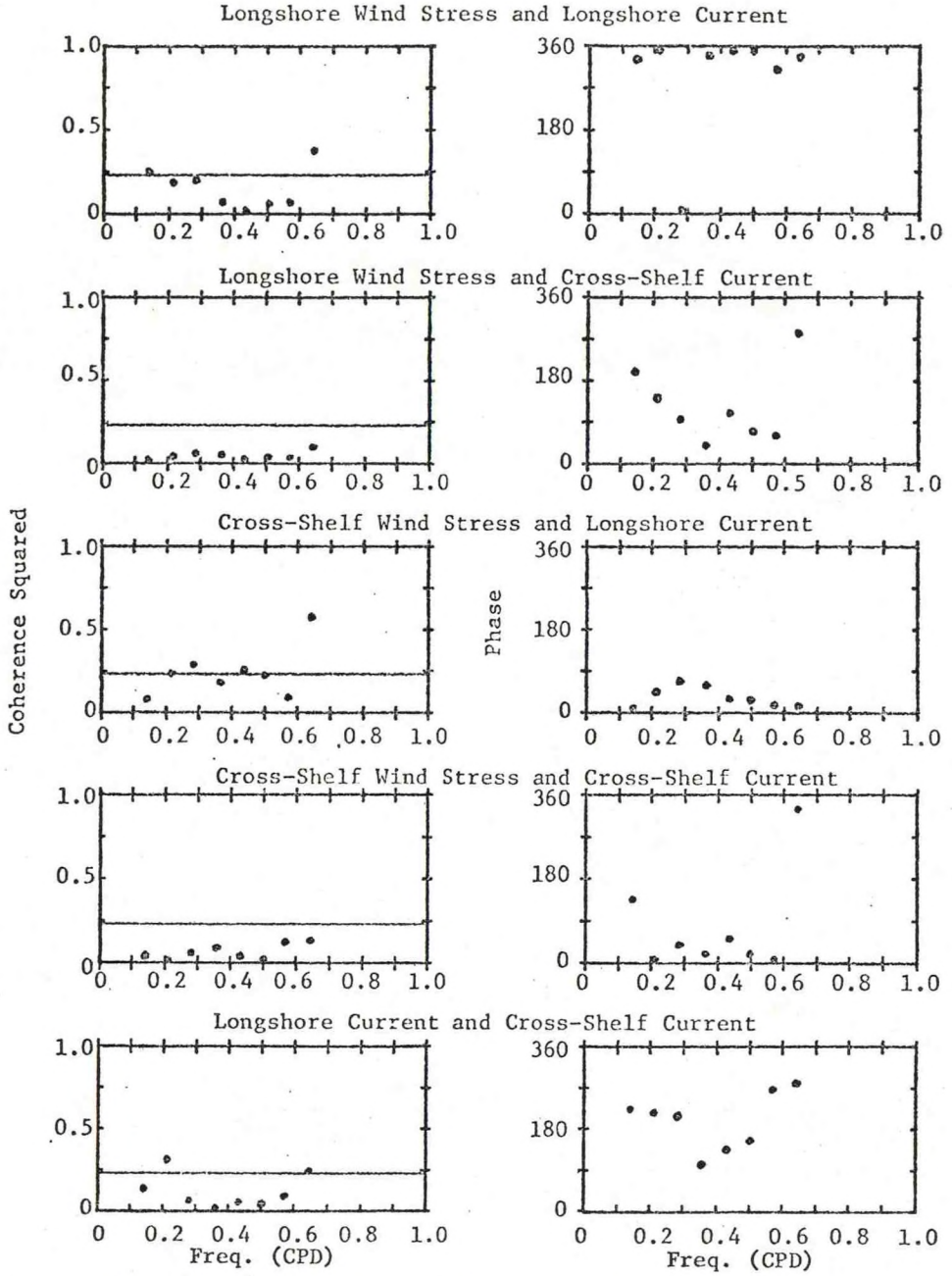

Figure I-28. Coherence squared and phase (in degrees) spectra between wind stress and surface current components for 18 October-31 December 1978. The line across the coherence squared is the 90% confidence limit, and the 95% confidence interval for the phases is ±46°. Larger coherence squared values will have smaller confidence intervals for the corresponding phase.

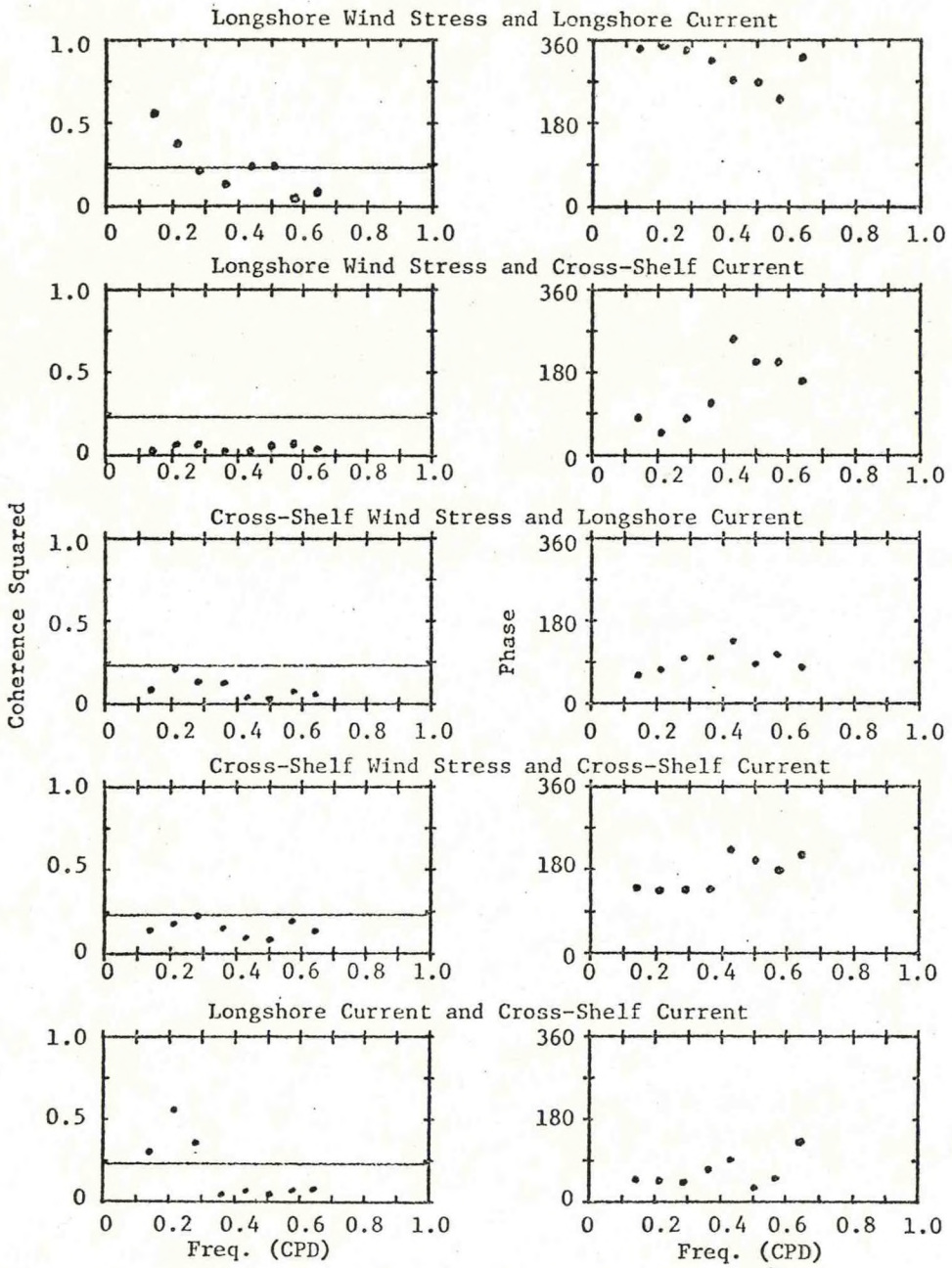

Figure I-29. Coherence squared and phase (in degrees) spectra between wind stress and bottom current components for 18 October-31 December 1978. The line across the coherence squared is the 90% confidence limit, and the 95% confidence interval for the phases is ±46°. Larger coherence squared values will have smaller confidence intervals for the corresponding phase.

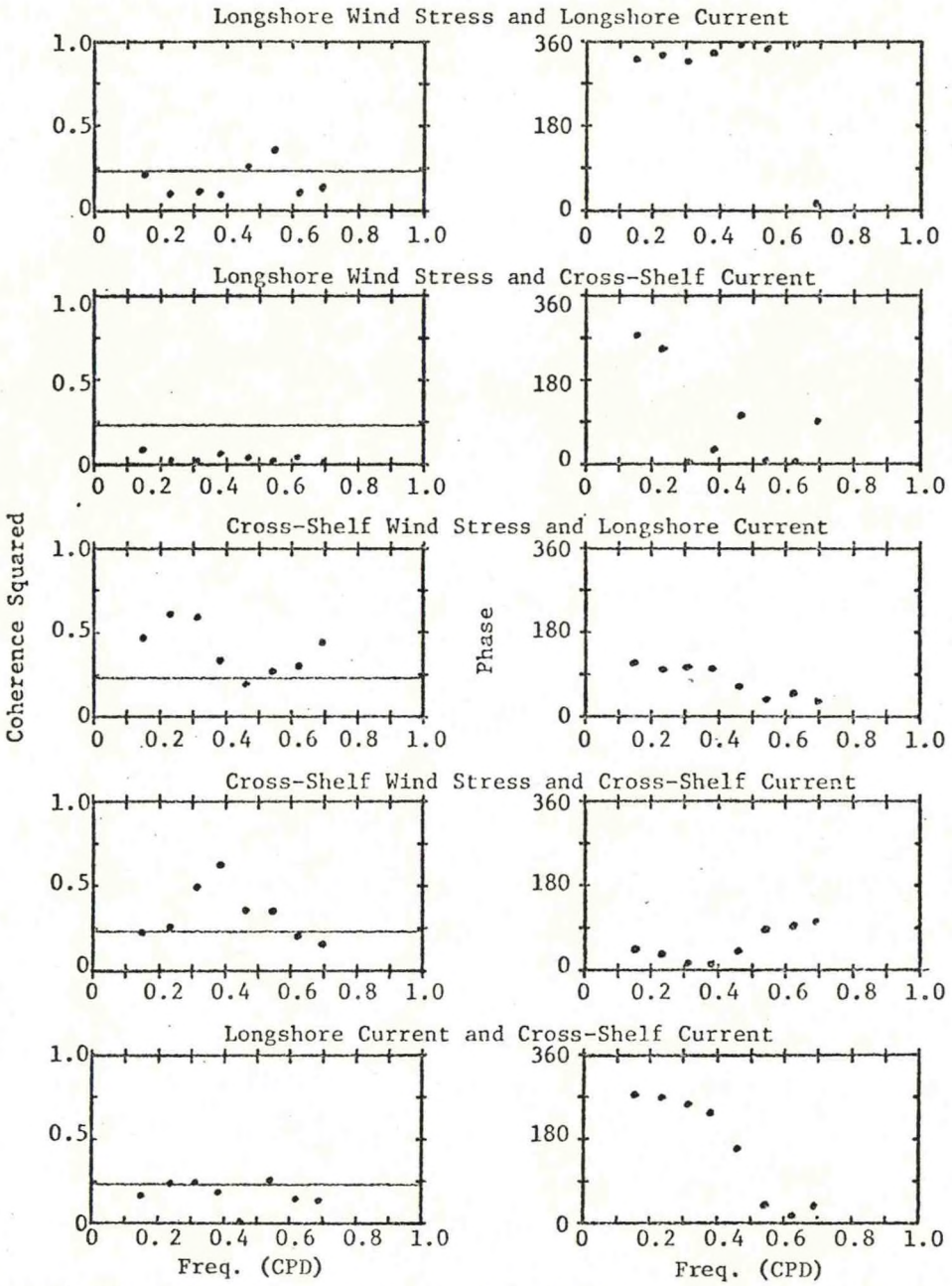

Figure I-30. Coherence squared and phase (in degrees) spectra between wind stress and surface current components for 30 November 1978-5 February 1979. The line across the coherence squared is the 90% confidence limit, and the 95% confidence interval for the phases is ±46°. Larges coherence squared values will have smaller confidence intervals for the corresponding phase.

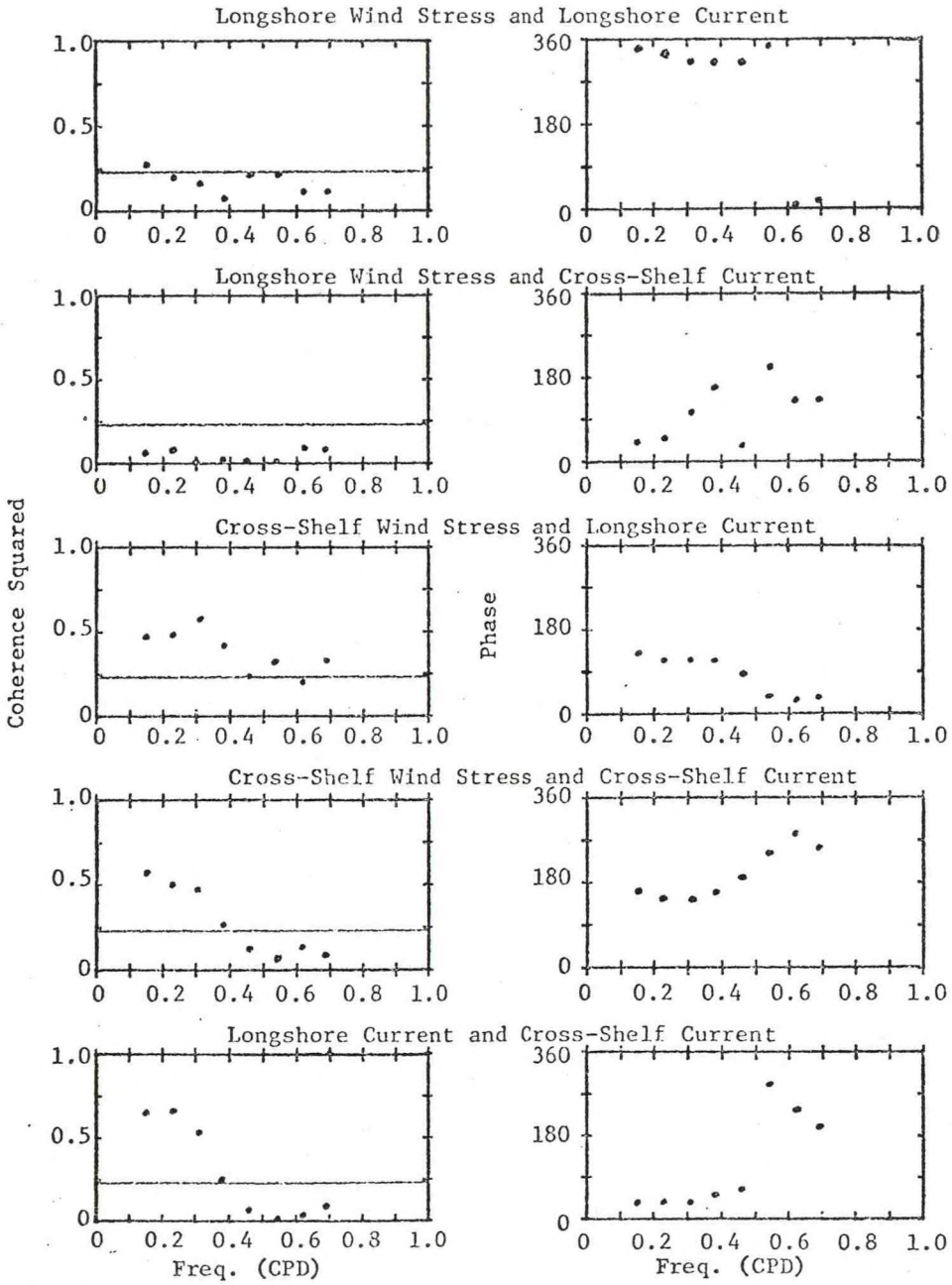

Figure I-31. Coherence squared and phase (in degrees) spectra between wind stress and bottom current components for 30 November 1978–5 February 1979. The line across the coherence squared is the 90% confidence limit, and the 95% confidence interval for the phase is ±46°. Larger coherence squared values will have smaller confidence intervals for the corresponding phase.

Time Period	Average Wind Speeds (m/s) Longshore	Cross-shelf
17 Oct.-17 Nov. 1977	0.2	1.2
18-31 Nov. 1977	-2.2	5.2
22-31 Dec. 1977	-3.2	1.4
20 Jan.- 3 Feb. 1978	-6.1	-3.1
4-25 Feb. 1978	-3.6	-2.5
26 Feb.-23 Mar. 1978	-0.8	0.3
24 Mar.-19 Apr. 1978	-1.6	3.0
20 Apr.-25 May 1978	-1.2	4.0
26 May-13 June 1978	-0.1	5.1
1-18 July 1978	2.7	2.8
19 July-30 Aug. 1978	0.4	3.1

Table I-1. Variations of the mean cross-shelf wind speed (positive is onshore) and mean longshore wind speed (positive is northeast) for periods between the hydrographic samplings from October 1977 through August 1978.

Time Period	Average Wind Speeds (m/s) Longshore	Cross-shelf
31 Aug.-30 Sept. 1978	-2.4	2.8
30 Sept.-31 Oct. 1978	-2.9	1.0
31 Oct.-30 Nov. 1978	-2.7	0.5
30 Nov.-31 Dec. 1978	-2.1	0.0
31 Dec. 1978-31 Jan 1979	-3.0	-2.0
31 Jan.-28 Feb. 1979	-2.9	-0.1

Table I-2. Variations of the mean cross-shelf wind speed (positive is onshore) and mean longshore wind speed (positive is northeast) for periods between 31 August 1978-28 February 1979.

Table I-3. Average currents and wind stresses for the designated periods during the study.

	$\bar{u}$ (cm/s)	$\bar{v}$ (cm/s)	$\bar{\tau}_x$ (dyn/cm^2)	$\bar{\tau}_y$ (dyn/cm^2)	Thermocline Status
	23 Dec - 25 Dec 1977, $u_T > 5$ cm/s, 60 hrs.				
Surface	26.1	-7.7	0.10	-0.12	Thermocline not present
Bottom	11.9	10.5			
	25 Dec - 30 Dec 1977, $u_T < -5$ cm/s, 120 hr.				
Surface	-32.5	13.6	-1.45	0.48	Thermocline not present
Bottom	-17.3	-9.7			
	17 Mar - 20 Mar 1978, $u_T > 5$ cm/s, 84 hrs.				
Surface	17.6	-5.7	0.06	0.18	Thermocline not present
Bottom	10.3	2.2			
	20 Mar - 21 Mar 1978, $0 < u_T \leq 5$ cm/s, 24 hrs.				
Surface	3.5	-7.5	-0.02	0.27	Thermocline not present
Bottom	-10.1	-1.6			
	21 Mar - 29 Mar 1978, $u_T < -5$ cm/s, 180 hrs.				
Surface	-18.8	0.9	-0.23	-0.27	Thermocline not present
Bottom	-5.2	-1.4			
	30 June - 30 June 1978, $0 < u_T \leq 5$ cm/s, 12 hrs.				
Surface	0.8	-2.8	0.22	0.22	Thermocline present
Bottom	-1.4	1.0			
	30 June - 16 July 1978, $u_T > 5$ cm/s, 384 hrs.				
Surface	20.5	-6.5	0.13	0.12	Thermocline present
Bottom	8.2	2.2			
	16 July - 20 July 1978, $u_T > 5$ cm/s, 96 hrs.				
Surface	20.9	8.4	0.06	0.09	Thermocline not present
Bottom	-1.7	1.7			
	20 July - 21 July 1978, $0 < u_T \leq 5$ cm/s, 12 hrs.				
Surface	2.9	9.8	-0.16	0.42	Thermocline not present
Bottom	-13.1	-8.2			
	21 July - 22 July 1978, $-5 \leq u_T < 0$ cm/s, 24 hrs.				
Surface	-2.5	9.5	-0.12	0.18	Thermocline not present
Bottom	-17.2	-13.4			

Table I-3. (continued)

	$\bar{u}$ (cm/s)	$\bar{v}$ (cm/s)	$\bar{\tau}_x$ (dyn/cm^2)	$\bar{\tau}_y$ (dyn/cm^2)	Thermocline Status
	22 July - 23 July 1978, u_T <-5 cm/s, 36 hrs.				
Surface	-14.0	7.1	-0.02	0.14	Thermocline not present
Bottom	-15.0	-9.7			
	23 July - 24 July 1978, $-5 \leq u_T < 0$ cm/s, 12 hrs.				
Surface	-0.4	2.8	0.16	0.21	Thermocline not present
Bottom	-5.9	0.6			
	24 July - 3 Aug 1978, $u_T > 5$ cm/s, 240 hrs.				
Surface	19.4	2.5	0.09	0.27	Thermocline not present
Bottom	7.2	1.8			
	3 Aug - 4 Aug 1978, $0 < u_T \leq 5$ cm/s, 24 hrs.				
Surface	3.2	11.0	-0.09	-0.01	Thermocline not present
Bottom	-5.9	-3.3			
	4 Aug - 9 Aug 1978, $-5 \leq u_T < 0$ cm/s, 120 hrs.				
Surface	-4.1	6.3	-0.05	0.02	Thermocline not present
Bottom	-10.4	-7.7			
	9 Aug - 18 Aug 1978, $u_T > 5$ cm/s, 228 hrs.				
Surface	23.1	-1.8	0.15	0.27	Thermocline not present
Bottom	8.7	3.2			
	18 Aug - 19 Aug 1978, $0 < u_T \leq 5$ cm/s, 12 hrs.				
Surface	4.7	-3.2	-0.05	0.09	Thermocline not present
Bottom	-6.4	-6.5			
	19 Aug - 3 Sept 1978, $u_T < -5$ cm/s, 348 hrs.				
Surface	-26.9	8.0	-0.09	0.10	Thermocline not present
Bottom	-12.0	-4.1			

Table I-4. A comparison of surface longshore currents as estimated from hydrographic data using the geostrophic assumption and of surface longshore currents for the same times as measured by current meters.

Date	Geostrophic Surface Longshore Current (cm/s)	Longshore Current (cm/s) from the Surface Current Meter
23 Mar 1978	-30	-26
25 Mar 1978	-30	-31
20 June 1978	-13	-18
21 June 1978	-27	-11
22 June 1978	-27	-9
18 July 1978	13	15
20 July 1978	20	25
30 Aug 1978	-34	-40
31 Aug 1978	-35	-35
1 Sept 1978	-44	-37

Table I-5

A comparison of theoretical phase shifts between a cross-shelf wind stress and surface and bottom current components with the average of statistically significant phase shifts between the winter cross-shelf wind stress and surface and bottom current components.

	Current Component			
	u_1	v_1	u_2	v_2
Theoretical	0°	-270°	-180°	-90°
Actual	-280°	-320°	-269°	-206°
Difference	+80°	-50°	-89°	-116°